ELSEVIER

Chemical Geology 234 (2006) 179–210

CHEMICAL GEOLOGY
INCLUDING
ISOTOPE GEOSCIENCE

www.elsevier.com/locate/chemgeo

Geochemistry of abyssal peridotites (Mid-Atlantic Ridge, 15°20′N, ODP Leg 209): Implications for fluid/rock interaction in slow spreading environments

H. Paulick [a,*], W. Bach [b,1], M. Godard [c], J.C.M. De Hoog [d], G. Suhr [e], J. Harvey [f]

[a] *Mineralogisch- Petrologisches Institut, Universität Bonn, Poppelsdorfer Schloss, 53115 Bonn, Germany*
[b] *Department of Marine Chemistry and Geochemistry, WHOI, 360 Woods Hole Road, Woods Hole, MA 02543, USA*
[c] *Laboratoire de Tectonophysique, Université Montpellier II, Case Courrier 49, Place Eugéne Bataillon, 34095 Montpellier cedex 5, France*
[d] *Institute for Earth Sciences, Göteborg University, Box 460, 405 30 Göteborg, Sweden*
[e] *Institut für Geologie und Mineralogie, Universität zu Köln, Zülpicher Street 49b, 50674, Köln, Germany*
[f] *Department of Earth Sciences, the Open University, Walton Hall, Milton Keynes, MK7 6AA, United Kingdom*

Received 3 December 2005; received in revised form 20 April 2006; accepted 27 April 2006

Abstract

Abyssal peridotite from the 15°20′N area of the Mid-Atlantic Ridge show complex geochemical variations among the different sites drilled during ODP Leg 209. Major element compositions indicate variable degrees of melt depletion and refertilization as well as local hydrothermal metasomatism. Strongest evidence for melt–rock interactions are correlated Light Rare Earth Element (LREE) and High Field Strength Element (HFSE) additions at Sites 1270 and 1271. In contrast, hydrothermal alteration at Sites 1274, 1272, and 1268 causes LREE mobility associated with minor HFSE variability, reflecting the low solubility of HFSE in aqueous solutions. Site 1274 contains the least-altered, highly refractory, peridotite with strong depletion in LREE and shows a gradual increase in the intensity of isochemical serpentinization; except for the addition of H_2O which causes a mass gain of up to 20 g/100 g. The formation of magnetite is reflected in decreasing Fe^{2+}/Fe^{3+} ratios. This style of alteration is referred to as rock-dominated serpentinization. In contrast, fluid-dominated serpentinization at Site 1268 is characterized by gains in sulfur and development of U-shaped REE pattern with strong positive Eu anomalies which are also characteristic for hot (350 to 400 °C) vent-type fluids discharging from black smoker fields. Serpentinites at Site 1268 were overprinted by talc alteration under static conditions due to interaction with high a_{SiO_2} fluids causing the development of smooth, LREE enriched patterns with pronounced negative Eu anomalies. These results show that hydrothermal fluid–peridotite and fluid–serpentinite interaction processes are an important factor regarding the budget of exchange processes between the lithosphere and the hydrosphere in slow spreading environments.

Keywords: Serpentinization; Slow spreading ridges; Abyssal peridotite; Hydrothermal alteration; Geochemistry; Ocean Drilling Program Leg 209

1. Introduction

Abyssal peridotites represent sections of the upper mantle which are exposed on the seafloor in and near fracture zones and along slow and ultraslow spreading ridges due to tectonic faulting associated with extension

* Corresponding author. Tel.: +49 228 736816.
E-mail address: Holger.Paulick@uni-bonn.de (H. Paulick).
[1] Current address: Universität Bremen, Fachbereich 5 - Geowissenschaften, Postfach 330 440, 28334 Bremen, Germany.

0009-2541/$ - see front matter © 2006 Elsevier B.V. All rights reserved.
doi:10.1016/j.chemgeo.2006.04.011

and crustal thinning. Current estimates indicate that ridges with a spreading rate of less than 20 mm yr^{-1} comprise about one third of the 55,000 km global ridge system (Dick et al., 2003). Prominent examples include the Southwest Indian Ridge (e.g., Sauter et al., 2004) the Gakkel Ridge in the Arctic ocean (e.g., Cochran et al., 2003) and segments of the Mid-Atlantic Ridge (MAR; Lagabrielle et al., 1998 and references therein). Hence, upper mantle rocks are important components of the shallow oceanic lithosphere and an integral part of hydrothermal interaction processes at divergent plate margins.

The significance of hydrothermal interaction processes involving ultramafic rock has become increasingly evident. It was realized that fluid–peridotite interaction has important consequences for the rheology of the oceanic lithosphere (Escartín et al., 1997), geochemical budgets of the oceans (Thompson and Melson, 1970; Snow and Dick, 1995) and microbial processes at and below the seafloor (Alt and Shanks, 1998; Kelley et al., 2005).

The most prominent manifestations of these processes are active, ultramafic hosted hydrothermal systems discharging hot (350 to 400 °C) metal-rich fluids and generating black smoker chimney fields on the seafloor (e.g., Logatchev and Rainbow Sites, Mozgova et al., 1999; Douville et al., 2002). Lower temperature (40–90 °C) hydrothermal venting has been recently discovered in the off axis environment (Lost City Hydrothermal Field, Kelley et al., 2001; Früh-Green et al., 2003; Kelley et al., 2005). On a larger scale, chemical (CH_4 and Mn) and turbidity anomalies in the water column along slow and ultraslow spreading ridges indicate that hydrothermal systems are common in this environment (Charlou et al., 1993; German et al., 1998; Edmonds et al., 2003). Some of these occurrences are clearly associated with avolcanic spreading (Bach et al., 2002), and others have high ratios of CH_4 to Mn (Charlou et al., 1993), indicating a significant contribution from peridotite-hosted hydrothermal systems.

In general, hydrothermal alteration of peridotite is inferred to be dominated by hydration reactions of olivine and pyroxene that lead to the formation of serpentine minerals ("serpentinization *senso stricto*"; e.g., Miyashiro et al., 1969; Wicks and Whittaker, 1977; Komor et al., 1985; Janecky and Seyfried, 1986; O'Hanley, 1996). However, Ocean Drilling Program (ODP) Leg 209 drill core of abyssal peridotite from five sites along the MAR in the 15°20′N area show a remarkable diversity of alteration intensities and mineral assemblages indicating that fluid–peridotite, and fluid–serpentinite, interaction can take place at a wider range of temperature and redox conditions than commonly appreciated (Figs. 1 and 2, Table 1; Bach et al., 2004).

The purpose of this paper is to investigate the geochemical systematics of these abyssal peridotite samples in order to determine the influence of hydrothermal alteration on their composition. Hence, this study contributes to the characterization of the geochemical budget of the lithosphere at slow and ultraslow spreading ridges.

1.1. Local geology and hydrothermal alteration of peridotite in the 15°20′N area

Abundant peridotite and gabbroic rocks are exposed on both flanks of the spreading axis of the slow spreading MAR to the north and south of the 15°20′N Fracture Zone (full rate: 25 mm yr^{-1}; Lagabrielle et al., 1998; Escartín et al., 2003; Kelemen et al., 2004). In this area, widespread fluid–peridotite interaction in the sub-seafloor is evident from extensive CH_4 and H_2 anomalies in the water column and high-*T* hydrothermal discharge at the active Logatchev black smoker field (Fig. 1; Batuev et al., 1994; Bogdanov et al., 1997; Charlou et al., 1998).

The ODP Leg 209 drill Sites 1268, 1270, 1271, 1272, and 1274 are located within the MAR axial valley and on the immediate valley walls between 14°40′N and 15°40′N and between 18 and 156 m of basement dominated by ultramafic rocks have been penetrated (Figs. 1 and 2 and Table 1). Overall, mantle deformation fabrics are weakly developed and deformation was localized along ductile shear zones formed under granulite to greenschist facies conditions and late brittle faults. Intact blocks of peridotite with protogranular fabrics were preserved between these zones and underwent tectonic rotation (Kelemen et al., 2004; Shipboard Scientific Party, 2004; Kelemen et al., submitted for publication).

Detailed accounts of the lithologies drilled during ODP Leg 209 are presented in the ODP Initial Results Volume (Shipboard Scientific Party, 2004). The style and intensity of hydrothermal alteration varies between the sites and the fluid–rock interaction processes are controlled by a variety of factors including reaction kinetics, temperature, modal mineralogy of the protolith, fluid composition, redox variations, and metasomatic processes (Bach et al., 2004). Here, we present a summary of the lithological characteristics and the principal controls on hydrothermal alteration in order to provide a framework for the interpretation of the geochemical variations.

Hole 1274A (Fig. 2A) contains the "least-altered" harzburgite and dunite. The intensity of serpentinization ranges from highly altered (~60 vol.% secondary minerals) in the upper part of the hole to completely altered (>95 vol.% secondary minerals) in the lower portion that is also characterized by abundant fault zones. Brucite–serpentine–magnetite is the common alteration

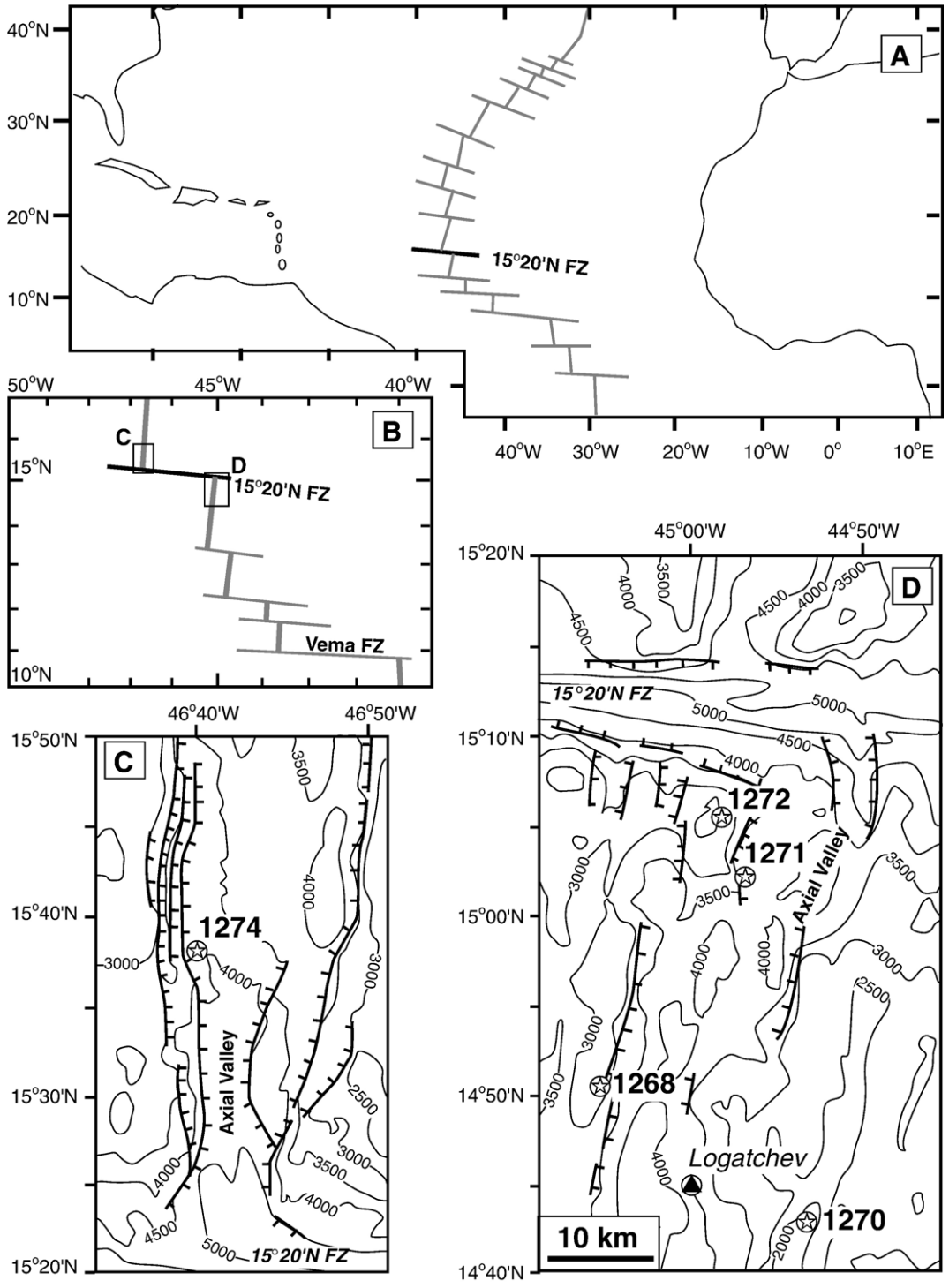

Fig. 1. ODP Leg 209 recovered variably altered peridotite at five sites in the vicinity of the 15°20′N Fracture Zone. A: Location of the 15°20′N Fracture Zone in the Atlantic Ocean. B: Location of the southern and northern working area of ODP Leg 209. C and D: Location of ODP Sites 1268, 1270, 1271, 1272, and 1274 (stars). The location of the Logatchev active hydrothermal site (triangle) is also shown. Bathymetry from Lagabrielle et al. (1998).

assemblage in dunite whereas brucite is rare in harzburgite. This indicates that brucite is stabilized in orthopyroxene-poor peridotite whereas formation of serpentine from orthopyroxene in harzburgite releases SiO_2 to the fluid promoting the reaction of brucite to serpentine (Bach et al., 2004). Late-stage interaction with ambient seawater is documented by aragonite veinlets and associated red halos of oxidative alteration (Fe-oxyhydroxide alteration). Variations in the $\delta^{18}O_{aragonite}$ indicate increasing formation temperatures from 2 °C near the seafloor to 15 °C at 90 mbsf (meter below sea-floor; Bach and Paulick, 2004).

The topmost ~50 m of Hole 1272A (Fig. 2B) consists of a diverse lithological assemblage including diabase, vesicular basalt, gabbro, serpentinized peridotite and carbonate-cemented breccia with serpentinite clasts which has been interpreted as a mega-breccia (Shipboard Scientific Party, 2004). Below this unit, serpentinized harzburgite with minor dunite consists of serpentine–magnetite±brucite±iowaite assemblages. Iowaite ($Mg_4[OH]_8Fe^{3+}OCl\times 1–4\ H_2O$) has been described previously from submarine mud volcanoes (Heling and Schwarz, 1992) and serpentinites at the Iberian margin (Gibson et al., 1996). Iowaite in Hole 1272A represents the first documented occurrence of this mineral in a mid-ocean ridge setting (Shipboard Scientific Party, 2004); however, the presence of iowaite veins in Hess Deep serpentinites is reported in Früh-Green et al. (2004). In Hole 1272A, iowaite formed under oxidizing conditions from Fe-bearing brucite during late-stage, low temperature alteration (Bach et al., 2004).

Holes 1271A and B (Fig. 2C) recovered a complex mixture of ultramafic and mafic lithologies including melt-impregnated (commonly amphibole-bearing) dunite, amphibole gabbro, troctolite, and gabbroic intrusions. In addition, the dunite contains abundant disseminated chromite as well as irregular veinlets and individual chromite pods (Shipboard Scientific Party, 2004). Petrographic evidence for melt–rock interaction includes mm- to sub mm-scale network-like veins, commonly forming rims around spinel crystals, which are now composed of chlorite. The serpentinization of dunite and minor harzburgite is dominated by serpentine–brucite–magnetite assemblages; however, relict olivine is common in amphibole-bearing assemblages.

Four holes were drilled at Site 1270 on the eastern rift valley wall (Fig. 1). Holes 1270C and 1270D are located immediately adjacent to each other whereas Holes 1270B and 1270A are located at ~300 m and ~500 m down slope to the west (Shipboard Scientific Party, 2004). Hole 1270A (Fig. 2D) consists of serpentinized harzburgite with minor dunite and Hole 1270B (Fig. 2E) consists of gabbro with minor, completely talc altered, harzburgite. Holes 1270C and D (Fig. 2F) consist of serpentinized harzburgite and dunite, however, relict olivine and orthopyroxene are locally preserved. In these less serpentinized areas, pyroxene is replaced by talc and tremolite whereas olivine is weakly serpentinized documenting an initial high-temperature alteration stage ($T>350$ to 400 °C) where replacement of pyroxene proceeds at higher rates than alteration of olivine (Allen and Seyfried, 2003; Bach et al., 2004). Furthermore, there are abundant gabbroic intrusions which are commonly the focus of intense ductile deformation. These shear zones were locally invaded by mafic and differentiated melts as well as fluids of hydrothermal and magmatic origin causing the formation of amphiboles, local occurrences of zircon and apatite (Shipboard Scientific Party, 2004).

Hole 1268A (Fig. 2G) contains serpentinized and talc altered harzburgite and dunite in the upper section whereas gabbronorite dominates below 105 mbsf. Here, serpentinites contain up to 3 vol.% pyrite, which is otherwise rare in the altered peridotite drilled during ODP Leg 209. Talc alteration of serpentinites is interpreted as the result of Si-metasomatism and fluids with high a_{SiO_2} could have

Fig. 2. Graphic logs for ODP drill holes from Sites 1274, 1272, 1271, 1270 and 1268. The columns show the recovery rate, lithological characteristics, and the intensity of alteration and veining. The distribution of primary and alteration minerals is highly variable. (A). Hole 1274A contains the least-altered peridotite with up to 50 vol.% olivine and pyroxene in the upper section, however, serpentinization is complete below 100 mbsf. (B). The topmost ~50 m of Hole 1272A are interpreted as a mega-breccia dominated by basalt and diabase (Shipboard Scientific Party, 2004) whereas the lower section consists of completely serpentinized harzburgite with abundant iowaite ($Mg_4[OH]_8Fe^{3+}OCl\times 1–4\ H_2O$). (C). Holes 1271A and 1271B are 75 m apart and recovered a complex mixture of serpentine–brucite–magnetite altered, chromite-bearing dunite and minor harzburgite. Furthermore, there are amphibole gabbro, troctolite, and gabbroic intrusions. Utramafic samples from these holes show textural evidence for melt–rock interaction on hand specimen and thin section scale. (D, E, and F). Four holes were drilled at Site 1270: Holes 1270C and 1270D are located immediately adjacent to each other whereas Holes 1270B and 1270A are located at ~300 m and ~500 m down slope to the west (Shipboard Scientific Party, 2004). Hole 1270A consists mainly of serpentinized harzburgite with occasional gabbroic intrusion whereas Hole 1270B consists of gabbro and gabbronorite with minor occurrences of completely talc altered harzburgite. Serpentinized peridotite in Holes 1270C and D are heavily intruded by gabbroic dikelets. (G). Hole 1268A recovered completely serpentinized peridotite associated with pyrite-bearing veinlets (up to 3 vol.%) that have been overprinted by pervasive talc alteration. Magnetite is generally absent in talc altered serpentinite. Abbreviations: Altn: Alteration; Amp: Amphibole; Bru: Brucite; Carb: Carbonate; Chl: Chlorite; Cr-sp: Cr-spinel; Fe-oxi: Fe-oxyhydroxide; Mt: Magnetite; Opx: Orthopyroxene; Py: Pyrite; Serp: Serpentine (lizardite and/or chrysotile). Depth in meter below seafloor (mbsf); recovery in % per core barrel.

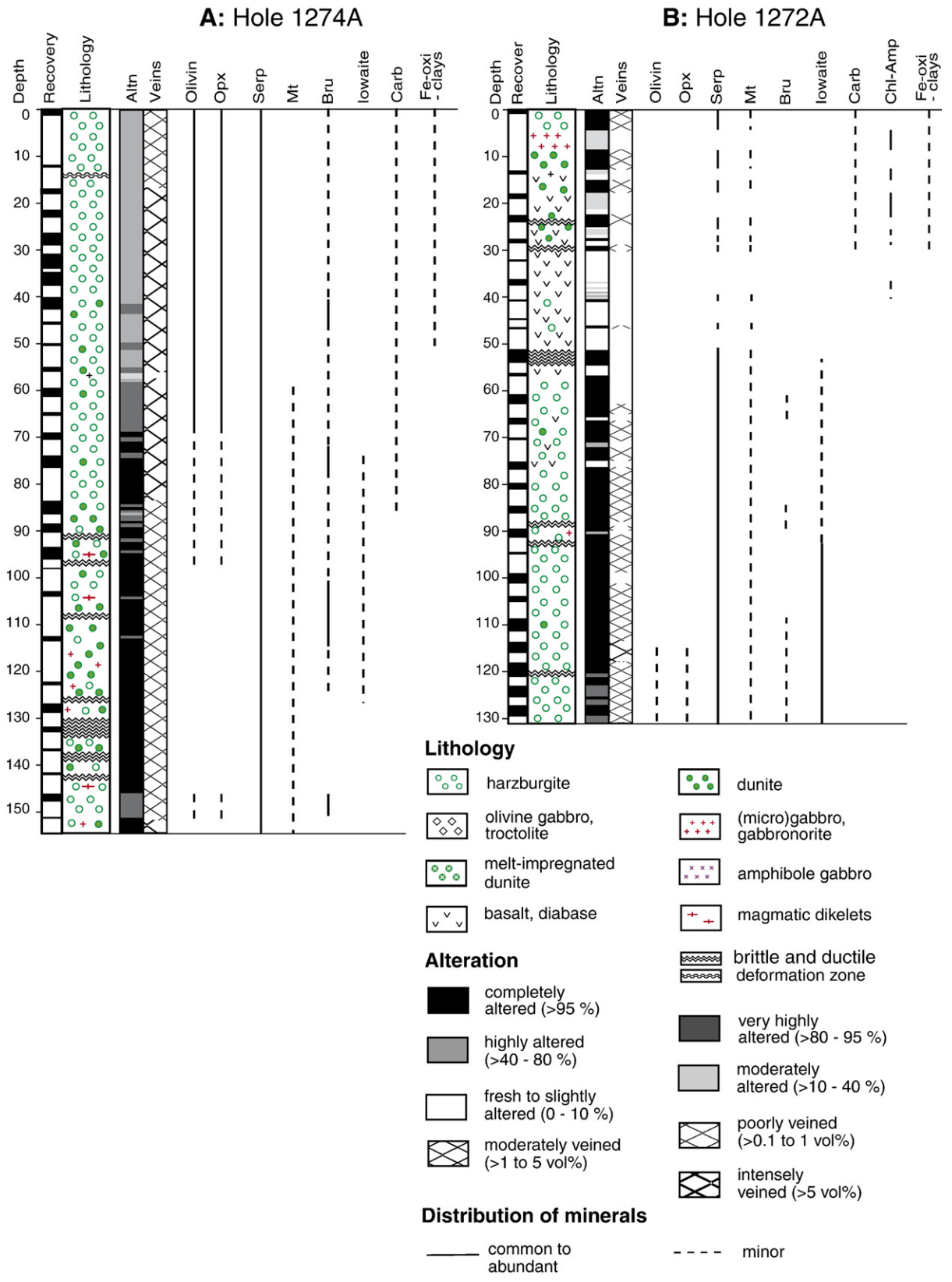
A: Hole 1274A
B: Hole 1272A
Depth
Recovery
Lithology
Altn
Veins
Olivin
Opx
Serp
Mt
Bru
Iowaite
Carb
Fe-oxi - clays
Chl-Amp
Lithology
harzburgite
olivine gabbro, troctolite
melt-impregnated dunite
basalt, diabase
dunite
(micro)gabbro, gabbronorite
amphibole gabbro
magmatic dikelets
brittle and ductile deformation zone
Alteration
completely altered (>95 %)
highly altered (>40 - 80 %)
fresh to slightly altered (0 - 10 %)
moderately veined (>1 to 5 vol%)
very highly altered (>80 - 95 %)
moderately altered (>10 - 40 %)
poorly veined (>0.1 to 1 vol%)
intensely veined (>5 vol%)
Distribution of minerals
common to abundant
minor

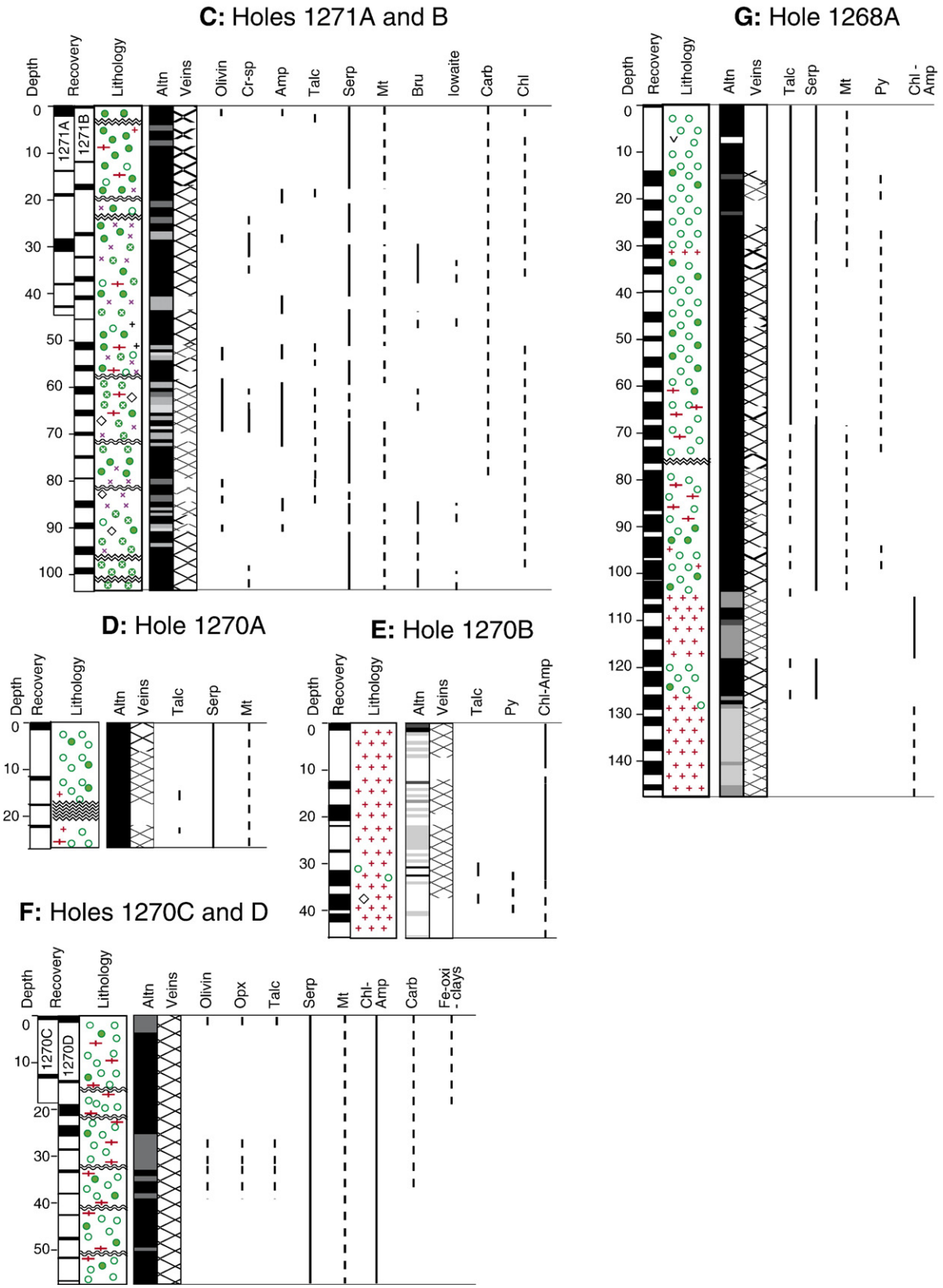

Fig. 2 (*continued*).

Table 1
Summary of drill holes, ODP Sites 1268, 1270, 1271, 1272, and 1274

Holes	1268A	1270A	1270B	1270C	1270D	1271A	1271B	1272A	1274A
Latitude	14°50.755′N	14°43.342′N	14°43.265′N	14°43.284′N	14°43.270′N	15°02.222′N	15°02.189′N	15°05.666′N	15°38.867′N
Longitude	45°04.641′W	44°53.321′W	44°53.225′W	44°53.091′W	44°53.084′W	44°56.887′W	44°56.912′W	44°58.300′W	46°40.582′W
Water depth (m)	3007	1951	1910	1822	1817	3612	3585	2560	3940
Basement penetration (m)	147.6	26.9	45.9	18.6	57.3	44.8	103.6	131.0	155.8
Core recovered (m)	78.7	3.3	17.2	2.0	7.7	5.8	15.9	37.5	34.7
Lithology									
Harzburgite	63%	89%	0.5%	81%	91%	1%	9%	93%	71%
Dunite	11%	5%	–	17%	7%	98%	56%	3.5%	19%
Gabbroic	26%	4%	99.5%	1%	2%	1%	35%	3.5%	3%
Fault gouge	–	2%	–	1%	–	–	–	–	7%
Alteration of peridotite	Serpentine, talc, pyrite, hematite, magnetite	Serpentine, magnetite	talc	Serpentine, magnetite	Serpentine, magnetite	Serpentine, brucite, magnetite	Serpentine, brucite, magnetite	Serpentine, iowaite, brucite, magnetite	Serpentine, brucite, magnetite
Veining	Talc, serpentine, sulfide, oxide	Serpentine, talc, magnetite	talc, chlorite, serpentine, amphibole, sulfide	Serpentine, oxide, talc, carbonate	Serpentine, oxide, talc, carbonate, sulfide, magnetite	Serpentine, talc, amphibole, magnetite, carbonate	Serpentine, magnetite, talc, carbonate, amphibole	Serpentine, carbonate, magnetite, clay	Serpentine, magnetite, carbonate
Abundance of metamorphic veins (%)	8.9	1.2	0.5	2.0	1.9	6.8	3.1	0.7	1.8
Alteration intensity (peridotite) (%)	98–100	98–100	100	98–100	50–100	30–100	30–100	90–100	30–100

Modified from Bach et al., 2004.

been derived from alteration of pyroxene in peridotite or gabbro at depth (Bach et al., 2004). Talc alteration occurred under static conditions as suggested by serpentinite microtextures that are perfectly pseudomorphed and preserved (Bach et al., 2004; Shipboard Scientific Party, 2004).

2. Methods

The geochemical data base consists of 168 analyses of peridotite drill core samples derived from ODP Sites 1268, 1270, 1271, 1272, and 1274. Examples of the typical rock types from these Sites are presented in Table 2. One group of 85 samples have been investigated on-board the JOIDES-Resolution during Leg 209 and have been analyzed for major and some trace elements by ICP-AES. Volatiles (H_2O, CO_2, and S) were determined by combustion and element analyses. These data and details of the analytical procedures are documented in Shipboard Scientific Party (2004).

A second set of 28 samples have been analyzed for major elements by XRF at the Open University (ARL 8420+) and volatile elements (CO_2, S, N) have been determined by elemental analyzers at GFZ-Potsdam. Whole rock trace element concentrations have been analyzed at the ISTEEM of Montpellier University (France) on a quadrupole VG-PQ2 Inductively Coupled Plasma-Mass Spectrometry (ICP-MS) following the procedure described in Ionov et al. (1992) and in Godard et al. (2000).

The method involves dissolution of 100 mg aliquots in a HF-$HClO_4$ mixture and dilution by a factor of 1000 for the analysis of trace elements, except for more concentrated elements such as Li, Cu, Ni, Co and Sc that were analyzed as a different batch with a dilution factor of 4000. In and Bi were used as internal standards during ICP-MS measurements. The REE, U, Th, Sr, Zr, Hf, Rb,

Table 2
Geochemical composition of variably altered peridotite from ODP Leg 209

Hole	1268A	1268A	1268A	1268A	1268A	1268A	1270D	1270D	1270D	1271A	1271B	1271B	1271B	1272A	1272A	1272A	1274A	1274A	1274A	1274A
Core	19	2	19	8	4	3	3	3	9	4	10	12	17	7	21	27	6	6	18	16
Section	1	2	3	1	3	1	2	2	1	2	1	1	1	1	1	2	2	3	1	2
Depth (cm)	34	108	6	28	26	29	39	85	44	5	30	46	61	116	27	12	128	24	83	26
Depth (mbsf)	97.3	16.48	99.88	44.3	28.04	20.49	20.6	21.01	47.84	29.8	50.8	60.6	85.1	38.1	99.17	128.62	32.73	33.1	94.13	85.4
Rock type	FD serp, Hz	FD serp, Hz	FD serp, Du	talc altn, Hz	talc altn, Hz	talc altn, Hz	serp Hz, MRI	serp Hz, MRI	serp Hz, MRI	serp Hz	serp Du, MRI	Gabbro	serp Du, MRI	Diabase	serp-iow Hz	serp-iow Hz	least-alt Hz	least-alt Hz	serp Hz	serp Du
Lab code	GR-06	AP-003	AP-023	GR-03	AP-008	AP-004	GR-09	AP-046	AP-050	GR-11	AP-063	GR-13	GR-15	GR-17	AP-077	AP-083	AP-086	GR-23	AP-096	GR-26
XRF Lab	OU	UB	UB	OU	UB	UB	OU	UB	UB	OU	UB	OU	OU	OU	UB	UB	UB	OU	UB	OU
[wt.%]																				
SiO_2	40.42	40.47	40.83	59.27	60.31	60.6	42.14	41.05	39.78	33.93	40.65	39.36	34.27	52.10	37.51	36.95	40.05	39.62	39.21	35.72
TiO_2	0.01	<0.01	<0.01	0.02	<0.01	<0.01	0.05	<0.01	<0.01	0.02	<0.01	0.07	0.01	1.48	<0.01	<0.01	<0.01	0.01	<0.01	0.01
Al_2O_3	0.44	0.68	0.56	0.90	0.6	0.35	1.34	0.98	0.48	0.61	0.56	3.90	0.19	15.36	0.61	0.53	0.71	0.64	0.99	0.20
Fe_2O_{3tot}	7.55	6.08	6.72	5.69	6.19	5.54	7.11	7.45	7.72	10.45	8.77	9.03	8.08	9.31	7.27	7.34	7.77	7.65	7.28	7.65
MgO	38.83	38.07	38.12	28.06	28.57	28.35	36.51	37.65	38.99	40.20	39.77	34.79	40.95	7.20	39.81	40.16	40.64	40.77	39.74	41.08
MnO	0.07	0.07	0.09	0.08	0.04	0.03	0.11	0.09	0.07	0.13	0.1	0.12	0.10	0.15	0.09	0.1	0.11	0.11	0.12	0.09
CaO	0.03	0.18	0.05	0.10	0.03	<0.02	0.48	0.15	<0.02	0.04	0.28	1.53	0.03	10.97	<0.02	0.05	0.77	0.85	0.52	0.13
Na_2O	0.08	0.1	0.1	0.24	0.16	0.16	0.16	0.13	0.14	0.06	0.17	0.46	0.06	2.62	0.17	0.11	0.05	0.05	0.06	0.06
K_2O	0.01	<0.01	<0.01	0.02	<0.01	<0.01	0.05	0.02	<0.01	0.03	<0.01	0.18	0.01	0.58	<0.01	<0.01	<0.01	0.01	<0.01	0.01
P_2O_5	0.01	0.01	<0.01	0.01	<0.01	<0.01	0.02	<0.01	0.01	0.01	<0.01	0.01	0.01	0.23	<0.01	<0.01	<0.01	0.01	<0.01	0.01
LOI	12.61	13.25	12.42	4.36	4.58	4.68	12.31	12.06	12.77	13.79	10.28	10.27	14.55	0.88	14.60	14.57	9.80	10.48	11.91	15.36
Total	100.06	98.91	98.89	98.74	100.48	99.71	100.28	99.58	99.96	99.27	100.58	99.73	98.26	100.88	100.06	99.81	99.90	100.19	99.83	100.31
FeO[a]	2.64	1.20	2.56	4.57	4.50	4.21	2.66	2.11	2.05	4.16	2.71	3.81	2.97	6.75	2.49	2.48	3.86	3.71	3.08	2.29
$Fe_2O_3^b$	4.62	4.74	3.87	0.61	1.19	0.86	4.15	5.10	5.44	5.83	5.76	4.80	4.78	1.81	4.50	4.58	3.48	3.53	3.86	5.10
Fe^{2+}ratio	0.39	0.22	0.42	0.89	0.81	0.84	0.42	0.32	0.30	0.44	0.34	0.47	0.41	0.81	0.38	0.38	0.55	0.54	0.47	0.33
CO_2	0.09	<0.45	<0.45	0.04	<0.45	<0.45	0.16	<0.45	<0.45	0.18	<0.45	0.27	0.21	0.25	<0.45	<0.45	<0.45	0.25	<0.45	0.36
S	0.21	2.09	0.65	0.13	0.24	0.18	0.05	0.04	0.05	0.14	0.05	0.07	0.20	0.10	0.21	0.18	0.04	0.07	0.08	0.15
N	bdl	<0.03	<0.03	bdl	<0.03	<0.03	0.009	<0.03	<0.03	0.002	<0.03	bdl	bdl	bdl	<0.03	<0.03	<0.03	0.002	<0.03	0.003
[ppm]																				
Cr_{XRF}	2005	3319	2236	2431	1736	1109	2469	2481	1753	6298	2549	4567	1813	284	2399	2013	2415	2427	3529	943
Ni_{XRF}	2138	2087	2102	1715	1634	1599	1999	1999	2350	2182	2249	1580	2549	97	2111	2163	2146	2134	2056	2453
ICP-MS Lab	UM	UG	UG	UM	UG	UG	UM	UG	UG	UM	UG	UM	UM	UM	UG	UG	UG	UM	UG	UM
Li	0.13	nd	nd	bdl	nd	nd	7.04	nd	nd	bdl	nd	3.40	11.00	3.20	nd	nd	nd	bdl	nd	0.04
Ba	0.04	3.44	0.58	0.10	bdl	2.11	6.22	3.48	bdl	0.83	3.89	8.29	0.13	113.94	3.14	2.27	1.24	0.14	1.12	0.001
Cs	0.002	<0.013	<0.013	0.002	<0.013	<0.013	0.011	<0.013	<0.013	0.002	0.016	0.021	bdl	0.099	<0.013	<0.013	0.016	0.001	<0.013	90
Co	96	92	106	91	79	75	93	98	114	121	111	143	45	50	100	98	97	97	100	108
Ni	2021	2029	2075	1589	1500	1534	1990	1994	2309	2020	2217	1580	253	124	2115	2094	2054	1930	2043	2273
As	nd	1.07	0.33	nd	0.45	0.40	nd	0.70	4.34	nd	1.26	nd	nd	nd	0.40	0.44	0.43	nd	0.49	nd
V	nd	29	22	nd	26	13	nd	35	23	nd	40	nd	nd	nd	21	18	31	nd	31	nd
Cr	nd	3006	1429	nd	1851	1126	nd	2420	1670	nd	2450	nd	nd	nd	1443	1319	1636	nd	2583	nd
Cu	13	15	35	11	546	82	4	3	5	6	4	4	3	67	6	6	6	8	6	13
Pb	0.24	7.79	0.59	0.11	0.32	0.37	0.03	0.13	0.16	0.05	0.23	0.15	0.27	0.86	0.17	0.06	bdl	bdl	bdl	0.06
Zn	nd	38	36	nd	100	66	nd	50	49	nd	61	nd	nd	nd	45	45	45	nd	45	nd
Sc	5.5	6.4	6.4	3.6	5.8	4.1	6.2	8.2	5.4	3.4	7.3	13.1	23.2	32.0	6.8	6.3	8.0	7.1	9.0	3.6
Rb	0.06	0.19	0.06	0.07	0.07	0.06	0.66	0.19	0.06	0.43	0.07	1.49	0.08	7.76	bdl	0.05	bdl	0.04	bdl	0.01
Sr	0.92	2.34	1.31	2.11	1.59	1.04	5.17	3.50	2.75	0.47	2.55	4.53	0.39	95.49	0.65	0.81	0.10	0.26	0.67	0.95
Y	0.06	0.13	0.04	1.52	1.48	0.84	3.28	2.23	0.44	0.10	0.38	2.15	0.47	23.37	0.03	0.02	0.11	0.10	0.10	0.08
Zr	bdl	0.58	0.09	0.93	0.66	3.20	5.07	0.87	3.38	0.25	0.29	1.52	0.84	125.96	0.10	0.09	0.06	bdl	0.10	0.05
Nb	0.01	0.05	0.02	0.07	0.05	0.08	3.94	0.79	0.23	0.15	0.07	0.10	0.06	19.68	0.01	0.01	0.01	0.01	0.01	0.01
Hf	0.00	<0.1	<0.1	0.02	<0.1	<0.1	0.18	<0.1	<0.1	0.01	<0.1	0.06	0.02	3.18	<0.1	<0.1	<0.1	0.00	<0.1	0.01
Ta	0.001	0.035	0.014	0.004	0.019	0.015	0.223	0.067	0.021	0.007	0.019	0.002	0.002	1.115	<0.005	0.005	<0.005	0.001	<0.005	0.001

Th	0.001	0.003	0.000	0.009	0.003	0.003	0.462	0.128	0.056	0.023	0.003	0.041	0.006	1.216	0.001	0.001	0.001	bdl	0.001	0.001
U	0.0009	0.0025	0.0025	0.0075	0.0025	0.0025	0.1968	0.8221	0.6360	0.0262	0.6362	0.1460	0.0065	0.3867	0.0511	0.0025	0.0025	bdl	0.0025	0.0014
La	0.0081	0.0760	0.0532	1.5309	0.4573	0.1805	2.3686	0.6516	0.3140	0.0430	0.1514	0.4250	0.0658	11.3345	0.0019	0.0014	0.0022	0.0004	0.0039	0.0017
Ce	0.0153	0.2044	0.0488	3.1947	1.2717	0.5349	5.0475	1.5654	0.8431	0.0677	0.3166	1.2277	0.2058	26.3415	0.0041	0.0025	0.0044	0.0024	0.0074	0.0031
Pr	0.0019	0.0267	0.0038	0.3276	0.1932	0.0780	0.5820	0.1952	0.0574	0.0073	0.0430	0.1737	0.0343	3.4116	0.0005	0.0003	0.0006	bdl	0.0007	0.0005
Nd	0.0062	0.1210	0.0116	1.2065	0.9556	0.4706	2.2942	0.8047	0.2085	0.0299	0.1697	0.7720	0.1869	15.5050	0.0016	0.0008	0.0017	0.0013	0.0036	0.0030
Sm	0.0043	0.0256	0.0012	0.2015	0.2526	0.1379	0.4716	0.2044	0.0390	0.0079	0.0396	0.2175	0.0596	3.7672	0.0005	0.0003	0.0010	0.0017	0.0012	0.0043
Eu	0.0215	0.0540	0.0562	0.0261	0.0112	0.0158	0.1452	0.0789	0.0206	0.0141	0.0209	0.1116	0.0295	1.2988	0.0004	0.0019	0.0003	bdl	0.0020	0.0019
Gd	0.0027	0.0161	0.0017	0.2190	0.2784	0.1766	0.5027	0.2771	0.0451	0.0095	0.0608	0.3044	0.0745	4.3021	0.0006	0.0003	0.0019	0.0022	0.0024	0.0091
Tb	0.0007	0.0019	0.0004	0.0329	0.0456	0.0242	0.0858	0.0465	0.0068	0.0018	0.0095	0.0578	0.0126	0.6893	0.0002	0.0001	0.0008	0.0007	0.0009	0.0019
Dy	bdl	0.0139	0.0044	0.2191	0.2796	0.1483	0.5834	0.3415	0.0495	0.0151	0.0688	0.4339	0.0875	4.5085	0.0019	0.0014	0.0100	0.0121	0.0092	0.0148
Ho	0.0028	0.0039	0.0014	0.0505	0.0560	0.0284	0.1229	0.0738	0.0119	0.0037	0.0145	0.0934	0.0187	0.9227	0.0012	0.0007	0.0038	0.0040	0.0036	0.0040
Er	0.0112	0.0163	0.0065	0.1457	0.1441	0.0767	0.3608	0.2369	0.0394	0.0131	0.0395	0.2645	0.0522	2.5732	0.0056	0.0042	0.0182	0.0182	0.0169	0.0129
Tm	0.0023	0.0030	0.0015	0.0196	0.0175	0.0119	0.0560	0.0377	0.0050	0.0031	0.0066	0.0413	0.0080	0.3637	0.0015	0.0012	0.0040	0.0038	0.0036	0.0020
Yb	0.0214	0.0199	0.0148	0.1141	0.1231	0.0707	0.3852	0.2525	0.0443	0.0321	0.0443	0.2670	0.0554	2.2780	0.0153	0.0126	0.0375	0.0346	0.0321	0.0149
Lu	0.0048	0.0032	0.0033	0.0171	0.0175	0.0123	0.0642	0.0424	0.0081	0.0085	0.0072	0.0450	0.0092	0.3643	0.0036	0.0032	0.0078	0.0077	0.0067	0.0031

Abbreviations: altn: alteration; bdl: below detection limit; FD serp: fluid-dominated serpentinization; Du: dunite; Hz: harzburgite; least-alt: least-altered; LOI: loss on ignition; MRI: melt–rock interaction REE signature; nd: not determined; serp: serpentinized; serp-iow Hz: iowaite-bearing serpentinized harzburgite.

Laboratories:

UB: University of Bonn; UG: University of Göteborg; UM: University of Montpellier; OU: Open University.

[a]FeO determined by titration.

[b]Fe_2O_3 recalculated from XRF and titration data.

Ba, Li, Cu, Ni, Co and Sc concentrations were determined by external calibration using multi element standard solutions (Merck). To avoid memory effects due to the introduction of concentrated Nb–Ta solutions in the instrument, Nb and Ta concentrations were determined by using, respectively, Zr and Hf as internal standards. This technique is an adaptation to ICP-MS analysis of the method described by Jochum et al. (1990) for the determination of Nb by spark-source mass spectrometry. The limits of detection, the procedural blank contributions and the values obtained for the international standards JP-1 and PCC-1 are reported in Table 3 (Appendix A).

A third set of 55 samples have been analyzed for major element concentrations by XRF at Bonn University (Philips PW1480) and volatiles (CO_2, S, N) have been determined at Freiberg University (VARIO EL gas analyzer). Trace and REE contents of these samples were determined by ICP-MS (HP4500 [Agilent] with Cetac ASX-500 autosample) at Göteborg University. About 100 mg of rock powder was digested using a HNO_3–HF mixture and diluted to a factor of 3800. Re and In were used as internal standards. Calibration was performed using four different multi element standards (Merck and Agilent). Accuracy was monitored using rock standards (JP-1, JB-1 and two in-house standards) treated as unknowns, and was within 10% for all analyzed except Hf and Ta (25%). Rocks that gave below-detection limit values for REE (28 samples) were re-analyzed for their REE content using an alternative procedure. Sample digestion was similar to the first method, instead that the final dilution factor was 500, and special care was taken to obtain low digestion blanks, including the use of ultra pure acids (Romil®) and pre-leached sample vials and bottles. To minimize matrix effects, a calibration standard was prepared by spiking an aliquot of one of the samples with a 100 ppb REE solution. Drift was monitored by analyzing JB-2 every four samples. This procedure allowed measuring REE concentrations of down to 0.001 chondrite. Reproducibility was measured on five duplicates and is on average 5%, but increases to 15% at element of <2.5 ppb in the sample. Rock standards JP-1, UB-N, NIM-D, NIM-P, NIM-N, and SARM47 were used to monitor accuracy and values are on average between 5 and 10% of literature values (Korotev, 1996; Makishima and Nakamura, 1997; Pin and Joannon, 1997).

In addition, the Fe^{2+} concentrations of 102 samples (second and third set, and shipboard samples of Hole 1268A) were determined by standard titration methods at the GeoForschungsZentrum Potsdam and Bonn University (Germany). The XRF, ICP-MS, volatile, and Fe^{2+} data of the second and third sets (83 samples) analyzed at

Table 3
Analyses of international standards at the universities of Montpellier (France) and Göteborg (Sweden)

	JP-1					PCC-1			NIM-N			LOD Montpellier	LOD Göteborg	Batch blanks Montpellier	Batch blanks Göteborg
	Average Montpellier	Standard Deviation	Average Göteborg	Standard Deviation	Preferred Values[a]	Average Montpellier	Standard Deviation	Preferred Values[b]	Average Göteborg	Standard Deviation	Preferred Values[c]				
N analyses	2		2			3			3					9	4
ppm															
Li	1.46		1.71		1.8	1.12		1.2	6		6	0.003	0.025	b.d.l	
Sc	6.37	0.06	6.57	0.13	7.24	7.1	0.4	8.4	39		39.8	0.001	0.014	b.d.l.	0.012
Ti	21.3	0.4	21.5			29	1	29	1152		1200	0.05	0.22	0.40	
Co	116	1	109	0	116	110	4	112	59		58	0.01	0.003	0.011	
Ni	2425	21	2302	15	2460	2325	80	2380	122		120	0.03	0.037	0.137	
V	na		20	0		na			224		220		0.013		
Cr	na		1576	20		na			29		30		0.37		
Cu	na		7	0		na			12		14		1.5		
Zn	na		45	1		na			61		68		0.31		
As	na		1	0		na			0.4				0.009		
Sn	na		0.026			na			0.7		1		0.05		
Sb	na		bdl			na			0.2		0.06		0.005		
ppb															
Rb	308	9	289	11	340	59	7	66	4191		4900	0.99	5.36	1.69	
Sr	662	75	<500		570	375	12	380	256,191		260,000	1.13	22.30	9.86	
Y	98	3	90	1	100	78	3	70	5150	216	6500	1.25	0.41	b.d.l	1.17
Zr	6039	442	6149	64	5340	128	10	134	11,550		23,000	1.51	6.89	6.51	
Nb	49	2	54	10	36	21.0	1.3	29	500		2000	0.39	1.08	0.39	
Cs	40	2	58	7	35	7.3	0.6	5.5	241		240	0.40	0.53	b.d.l	
Ba	11,514	605	10,345	54	9800	1468	89	900	82,178		84,000	1.22	194	177	
La	38	10	28		30	28.9	1.0	35	2878	150	2840	0.44	0.12	0.54	0.57
Ce	76	19	60		54	52.5	1.2	72	5912	261	5610	0.20	0.41	0.89	1.27
Pr	10	2	8		7.1	7.3	0.4	8.6	736	36	710	0.15	0.04	0.17	0.19
Nd	38	9	34		33	26.7	1.4	35	3301	139	3000	0.83	0.25	1.79	0.89
Sm	11	2	8		13	6.2	0.9	6.6	814	32	836	0.96	0.25	b.d.l	1.04
Eu	1.89	0.04	3.27		3.1	1.0	0.1	1.2	583	22	588	0.28	0.03	b.d.l	0.21
Gd	10.2	0.7	11.4		13	6.16	1.07	8.66	943	33	940	0.63	0.09	b.d.l	0.64
Tb	2.1	0.1	2.0		2.6	1.15	0.03	2	156	5	164	0.12	0.01	b.d.l	0.10
Dy	18.3	2.5	13.6		18	11.3	0.7	11	1027	35	1100	0.54	0.14	0.60	0.42
Ho	4.2	0.5	3.1		4.3	3.2	0.1	3	217	7	240	0.09	0.02	b.d.l	0.11
Er	13.9	0.9	12.0		14	11.95	0.97	12	632	21	660	0.72	0.24	b.d.l	0.49
Tm	2.5	0.1	2.1		2.7	2.54	0.17	2.87	94	2	99	0.21	0.04	b.d.l	0.10
Yb	21.7	1.5	20.1		21	22.8	1.3	24	641	16	656	0.48	0.18	b.d.l	0.56
Lu	4.6	0.3	4.2		4.7	5.2	0.3	5.7	96	2	101	0.21	0.02	b.d.l	0.11
Hf	143	6	317	155	120	4.2	0.3	6	495		360	0.47	0.98	b.d.l	
Ta	4.3	0.2	68.0	21.9	3.6	1.2	0.3	1.8	102		64	0.19	0.28	b.d.l	

Pb	78	7	na	80	90	8043	184	8500	na		7000	1.94		21.7	
Th	14	1	12	14	12	10.9	0.2	10	304	5	340	0.16	0.17	b.d.l	0.43
U	13.0	0.4		15.5	12	4.5	0.4	4.3	264		400	0.17	0.63	b.d.l	

Abbreviations: b.d.l.: below detection limit; LOD: Limit of detection; na: not analyzed.
Preferred values [a]: after Govindaraju (1994) and Godard et al. (2000); Preferred Values [b]: after Govindaraju (1994) and Takazawa et al. (2003); Preferred Values [c]: after Govindaraju (1994) and Korotev (1996).

References: Godard, M., Jousselin, D. and Bodinier, J.-L., 2000. Relationships between geochemistry and structure beneath a palaeo-spreading centre: a study of the mantle section in the Oman Ophiolite. Earth Planet. Sci. Lett., 180, 133–148.
Govindaraju, K., 1994. 1994 compilation of working values and sample description for 383 geostandards. Geostandards Newsletter, 18(Sp. Issue), 1–158.
Takazawa, E., Okayasu, T. and Satoh, K., 2003. Geochemistry and origin of the basal lherzolites from the northern Oman ophiolite (northern Fizh block). Geochem. Geophys. Geosyst., 4(2), 1021, doi:10.1029/2001GC000232.

the Universities of Bonn, Montpellier, Göteborg, the Open University, and GFZ Potsdam are documented in an electronic supplement to this paper (Supplementary Table).

The composition of the primary phases has been determined by electron microprobe analysis at the University of Köln (JEOL JXA-8900RL Superprobe; acceleration voltage: 20 kV for olivine and 15 kV for other phases; beam current: 50 nA for olivine and 20 nA for other phases; focused beam). In total, about 440 individual analyses have been obtained from 13 samples of Hole 1274A. These data are documented in a report to the ODP Scientific Results Volume for Leg 209 (Moll et al., submitted for publication). Furthermore, point counting data were obtained from the Hole 1274A samples, in order to constrain the modal proportions of mineral phases (1000 points on a 0.2×0.2 mm grid). These results were combined with the microprobe data in order to determine the protolith composition of the samples prior to serpentinization (Table 4).

3. Results

In MgO/SiO_2 vs. Al_2O_3/SiO_2 space (Fig. 3) a 'terrestrial array' represents the successive magmatic depletion of a primitive mantle and highly depleted compositions are characterized by low Al_2O_3/SiO_2 values (<0.01; Jagoutz et al., 1979; Hart and Zindler, 1986). A global data set of abyssal peridotite presented by Niu (2004) shows that these samples follow a similar trend that is systematically off set to lower MgO/SiO_2 values due to MgO loss during seafloor weathering (Snow and Dick, 1995; Niu, 2004). The increasing Al_2O_3/SiO_2 with decreasing MgO/SiO_2 in this data set are at least partially attributable to melt impregnation processes within the thermal boundary layer (Niu, 2004).

The drilled peridotites from the 15°20′N area show a considerable compositional diversity in MgO/SiO_2 vs. Al_2O_3/SiO_2 space that is related to a number of different processes. Similar to the most refractory peridotites from oceanic environments (Bodinier and Godard, 2003), most peridotites are strongly melt-depleted with low Al_2O_3/SiO_2 values (<0.02). Harzburgites from Holes 1272A and 1274A cluster tightly around the melting trend and preserve the high MgO/SiO_2 ratios typical of refractory mantle rocks (>1). However, most dunites from Hole 1274A and from Site 1271 plot systematically above the mantle array since their ratio of $olivine_{modal}/(olivine_{modal}+pyroxene_{modal})$ is close to 1. This compositional trend is well-known from ophiolitic and orogenic massifs (e.g., Godard et al., 2000). $Al_2O_3/$

Table 4
Hole 1274A — reconstructed primary mineralogy, composition, and mass change during serpentinization

Hole	1274A	1274A	1274A	1274A	1274A	1274A	1274A	1274A	1274A	1274A	1274A	1274A	1274A
Core	3	6	10	12	14	15	15	16	17	18	20	22	27
Section	1	2	1	1	1	1	2	1	1	1	1	1	2
Top (cm)	111	128	3	134	30	106	39	44	121	83	121	24	5
Bottom (cm)	120	135	10	142	36	114	46	52	129	93	126	32	11
Depth (mbsf)	18.01	32.73	49.93	60.74	69.3	75.06	75.86	84.14	89.51	94.13	104.11	122.34	147.65
Piece #	9	4	2	10	5	15A	5	7	21	15	23	4	2
Rocktype	least-alt Hz	least-alt Hz	serp Du	serp Hz	serp Hz	serp Du	serp Hz	serp Du	serp Hz	serp Hz	serp Du	serp Hz	serp Hz
Modal data [vol.%]													
Olivine	20.6	20	7.6	2.2	5.2	0.4	3.1	2.1	7.3	4.1	0	4.6	2.9
Orthopyroxene	13.4	8.3	0.3	1.5	3.9	0.1	1	0.6	0.9	1.5	0	5.3	1.4
Clinopyroxene	0.3	0.6	0.2	1.2	2.1	0.7	0.8	1.3	2.2	0.5	0	0.2	0.7
Spinel	1.6	0.3	1.2	0.5	0.1	1.3	1.5	0.2	1.6	1.3	0	0.7	0.1
Magnetite	0.9	1.8	9.6	2.6	3.7	13.4	7	6.9	10.4	0.2	1.5	0.5	1.5
Serp after ol	30	28.8	25	36.4	25.4	22.6	24.9	21.5	27.7	23.5	0	23.8	10.8
Brucite after ol	9.8	9.7	29.5	22.5	17.2	24.1	23.7	24	9.2	15.3	53.5	8.8	39
Serp after opx	16.7	12.1	0.7	7.8	15.5	8.7	11.4	14.3	18.9	12.7	0	20.7	16.6
Serp, origin?[a]	0	3.6	1.1	1.1	3	2.7	0	0	0	0	0	0	0
Serp in vein	6.3	11.9	17.1	18.9	19.6	17.1	20.9	14.3	10.8	27.9	30	34.6	22.1
Mgt in vein	0.4	2.9	7.9	5.3	4.3	8.9	5.7	11.3	11	15	13	0.8	4.9
Total:	100	100	100	100	100	100	100	100	100	100	100	100	100
Prim mineral[b]													
Total olivine	65.37	73.31	96.58	84.74	68.88	81.35	77.86	74.38	65.19	72.84	100.00	58.03	73.71
Total opx	32.58	25.56	1.56	12.90	27.95	15.20	18.67	23.28	29.20	24.11	0.00	40.56	25.17
cpx	0.32	0.75	0.20	1.66	3.03	1.21	1.20	2.03	3.24	0.85	0.00	0.31	0.98
Spinel	1.73	0.38	1.87	0.69	0.14	2.25	2.26	0.31	2.36	2.21	0.00	1.09	0.14
Total	100.00	100.00	100.00	100.00	100.00	100.00	100.00	100.00	100.00	100.00	100.00	100.00	100.00
n EMP[c]													
Olivine	18	17	20	13	15	23	1	16	16	14	1	17	9
Orthopyroxene	9	8	4	7	4	2	7	4	5	5	0	8	5
Clinopyroxene	9	13	8	16	6	9	14	12	15	10	0	5	3
Spinel	7	5	8	3	8	6	4	7	5	8	4	4	7
Reconst comp[d] [wt.%]													
SiO_2	44.58	44.27	40.29	42.39	45.15	42.24	43.93	44.45	44.57	43.47	40.25	46.61	44.54
TiO_2	0.01	0.01	0.00	0.01	0.02	0.01	0.05	0.03	0.01	0.01	0.00	0.01	0.01
Al_2O_3	1.40	0.81	0.39	0.64	0.87	0.82	0.98	0.69	1.39	1.18	0.14	1.29	0.76
Cr_2O_3	0.97	0.38	1.09	0.42	0.31	1.15	1.30	0.36	1.27	0.99	0.22	0.84	0.30
FeO_{tot}	7.34	7.63	7.72	7.88	7.30	8.06	8.06	7.61	7.24	7.79	8.93	6.67	7.46
MgO	43.92	45.91	50.14	47.89	44.92	47.03	44.80	45.86	44.01	45.75	50.16	43.75	46.04
MnO	0.13	0.13	0.07	0.13	0.13	0.11	0.18	0.12	0.13	0.13	0.13	0.13	0.13
CaO	1.64	0.85	0.29	0.64	1.28	0.56	0.69	0.85	1.38	0.68	0.17	0.67	0.74
Na_2O	0.01	0.00	0.00	0.00	0.01	0.01	0.01	0.04	0.01	0.01	0.00	0.02	0.01
K_2O	0.00	0.00	0.00	0.00	0.00	0.00	0.00	0.00	0.00	0.00	0.00	0.00	0.00

Total	100.00	100.00	100.00	100.00	100.00	100.00	100.00	100.00	100.00	100.00	100.00	100.00	100.00
Altered rock[e]													
SiO_2	39.43	40.12	35.11	37.82	38.69	35.67	37.60	37.22	39.08	39.15	35.40	38.54	37.59
TiO_2	0.01	0.01	0.00	0.01	0.02	0.01	0.01	0.02	0.01	0.00	0.01	0.00	0.00
Al_2O_3	0.67	0.71	0.30	0.65	0.69	0.22	0.49	0.40	0.87	0.99	0.10	0.70	0.66
Cr_2O_3	0.60	0.71	0.74	0.63	0.64	0.37	0.80	0.59	1.25	1.03	0.19	0.92	0.81
FeO_{tot}	7.09	7.00	7.28	6.68	6.81	7.08	6.85	7.02	6.56	6.54	7.40	6.17	6.70
MgO	41.58	40.71	42.61	39.89	40.10	41.30	40.43	40.47	39.82	39.68	41.41	39.85	40.22
MnO	0.11	0.11	0.11	0.11	0.11	0.10	0.10	0.09	0.12	0.12	0.10	0.10	0.10
CaO	0.55	0.77	0.18	0.50	0.53	0.17	0.43	0.39	0.73	0.52	0.02	0.21	0.35
Na_2O	0.07	0.05	0.06	0.09	0.08	0.08	0.09	0.06	0.04	0.06	0.08	0.10	0.08
K_2O	0.01	0.01	0.00	0.01	0.01	0.01	0.01	0.01	0.01	0.00	0.01	0.00	0.00
LOI	9.88	9.81	13.60	13.62	12.32	15.00	13.21	13.73	11.51	11.90	15.29	13.40	13.48
Total	100.00	100.00	100.00	100.00	100.00	100.00	100.00	100.00	100.00	100.00	100.00	100.00	100.00
EF values[f]													
EF_{SiO_2}	0.88	0.91	0.87	0.89	0.86	0.84	0.86	0.84	0.88	0.90	0.88	0.83	0.84
EF_{MgO}	0.95	0.89	0.85	0.83	0.89	0.88	0.90	0.88	0.90	0.87	0.83	0.91	0.87
$EF_{FeO_{tot}}$	0.97	0.92	0.94	0.85	0.93	0.88	0.85	0.92	0.91	0.84	0.83	0.93	0.90
$EF_{Al_2O_3}$	0.48	0.88	0.77	1.02	0.79	0.27	0.50	0.58	0.63	0.84	0.70	0.54	0.87
Average EF[g]	0.93	0.90	0.89	0.86	0.89	0.87	0.87	0.88	0.90	0.87	0.84	0.89	0.87
Total mass change [g/100 g]	7.24	10.70	12.61	16.58	11.83	15.33	15.06	13.53	11.59	15.03	18.43	12.67	14.70

Abbreviations: cpx: clinopyroxene; Du: dunite; EF: enrichment factor; EMP: electron microprobe; Hz: harzburgite; least-alt: least-altered; mgt: magnetite; ol: olivine; opx: orthopyroxene; prim mineral: primary mineralogy; reconst comp: reconstituted composition; serp: serpentinized; tot: total.

For the modal data, 1000 points have been counted in the thin sections on a 0.2×0.2 mm grid.

[a] Serpentinization of uncertain precursor.

[b] Modal proportions of primary minerals (excluding vein material and serpentinization of unknown origin). Total olivine includes serpentinization after olivine. Total orthopyroxene includes serpentinization after orthopyroxene.

[c] Number of microprobe analyses of primary phases. These analytical data are documented in a data report to the Ocean Drilling Program Leg 209 Scientific Results volume (Moll et al., submitted for publication).

[d] The geochemistry of the precursors has been reconstructed by combining the modal proportions of the primary phases and their composition (averages of the microprobe analyses).

[e] Normalized composition of the altered rock (analytical data documented in Supplementary Table).

[f] Enrichment factors calculated for SiO_2, MgO, FeO_{tot}, and Al_2O_3. Assumptions and procedures involved in this calculation are discussed in the text.

[g] Average enrichment factor based on EF_{SiO2}, EF_{MgO}, and EF_{FeOtot}.

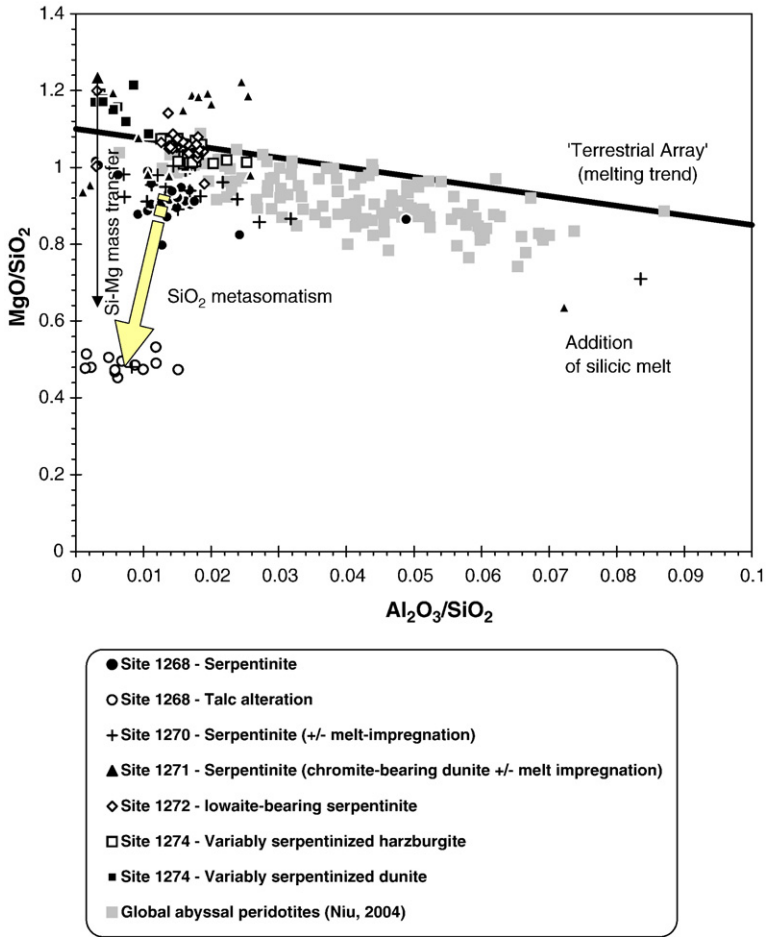

Fig. 3. In MgO/SiO_2 vs. Al_2O_3/SiO_2 space the data of the abyssal peridotite from the 15°20′N area show a considerable variability whereas analyses of a global set of abyssal peridotite presented by Niu (2004) define a trend parallel to the terrestrial array (Jagoutz et al., 1979). The geochemistry of the 15°20′N samples is controlled by a variety of processes including modal mineralogical composition and hydrothermal alteration.

SiO_2 values >0.02 at MgO/SiO_2 values around 1.2 (corresponding to Fo_{90} olivine) in dunites from Site 1271 are likely due to the addition of chromite. In contrast to these melt–rock interaction trends, serpentinized dunites and harzburgites of Sites 1268 and 1270 have MgO/SiO_2 values below the terrestrial array (0.8 to 1). These cannot be the result of melt–rock interaction but are either due to MgO loss during interaction with seawater or addition of silica. Talc alteration of serpentinites at Hole 1268A causes a further decrease in MgO/SiO_2 ratios that is likely due to Si-metasomatism, as will be discussed later.

3.1. Sites 1274 and 1272

Peridotites from Sites 1272 and 1274 have low concentrations in elements such as Al (Al_2O_3: 0.1 to 1 wt.%), Sc (2 to 9 ppm), and V (5 to 40 ppm; Fig. 4A and B) and are highly depleted in LREE with concentrations below 1% of the chondritic values whereas HREE concentrations are gradually increasing from Gd to Lu reaching Lu_N values of 0.3 (Fig. 5A and B). These compositions are similar to those observed in the most depleted peridotites sampled in oceans and ophiolitic massifs (Niu and Hekinian, 1997; Parkinson and Pearce, 1998; Pearce

Fig. 4. Major and trace element concentrations in variably altered peridotite recovered from ODP Sites 1268, 1270, 1271, 1272, and 1274. Major element concentrations are recalculated to 100% anhydrous. Symbols as in Fig. 3. (A). Al_2O_3 vs. V (B). Al_2O_3 vs. Sc (C). Al_2O_3 vs. Cr (D). Al_2O_3 vs. FeO_{total} (E). Al_2O_3 vs. modal proportion of pyroxene at Site 1274A (point counting data: modal pyroxene is preserved pyroxene+pyroxene pseudomorphed by serpentine; modal olivine is preserved olivine+olivine replaced by serpentine) (F). Al_2O_3 vs. MgO (G). Al_2O_3 vs. SiO_2.

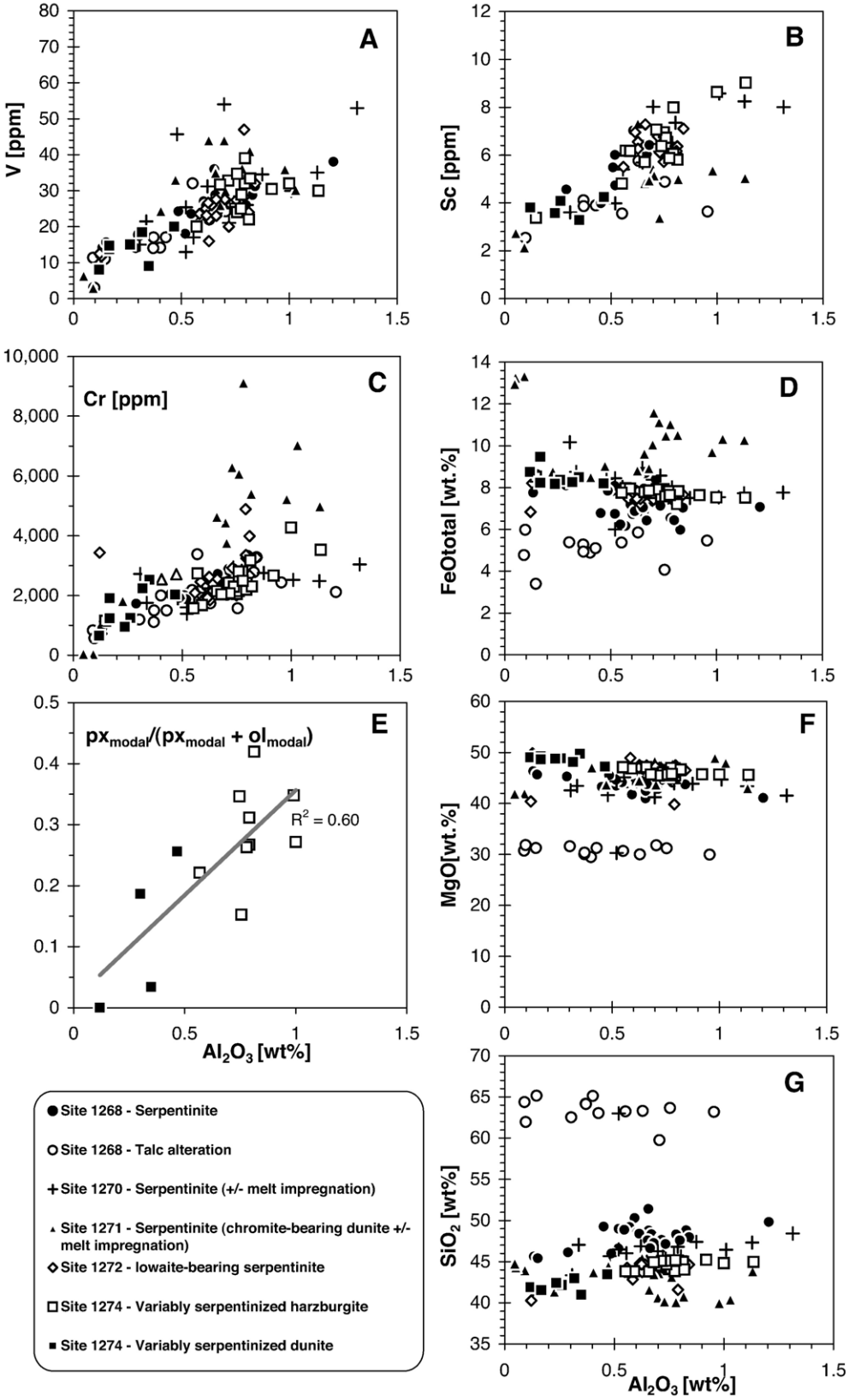
A
V [ppm]
B
Sc [ppm]
C
Cr [ppm]
D
FeOtotal [wt.%]
E
$px_{modal}/(px_{modal} + ol_{modal})$
$R^2 = 0.60$
Al_2O_3 [wt%]
F
MgO[wt.%]
G
SiO_2 [wt%]
Al_2O_3 [wt%]
Site 1268 - Serpentinite
Site 1268 - Talc alteration
Site 1270 - Serpentinite (+/- melt impregnation)
Site 1271 - Serpentinite (chromite-bearing dunite +/- melt impregnation)
Site 1272 - lowaite-bearing serpentinite
Site 1274 - Variably serpentinized harzburgite
Site 1274 - Variably serpentinized dunite

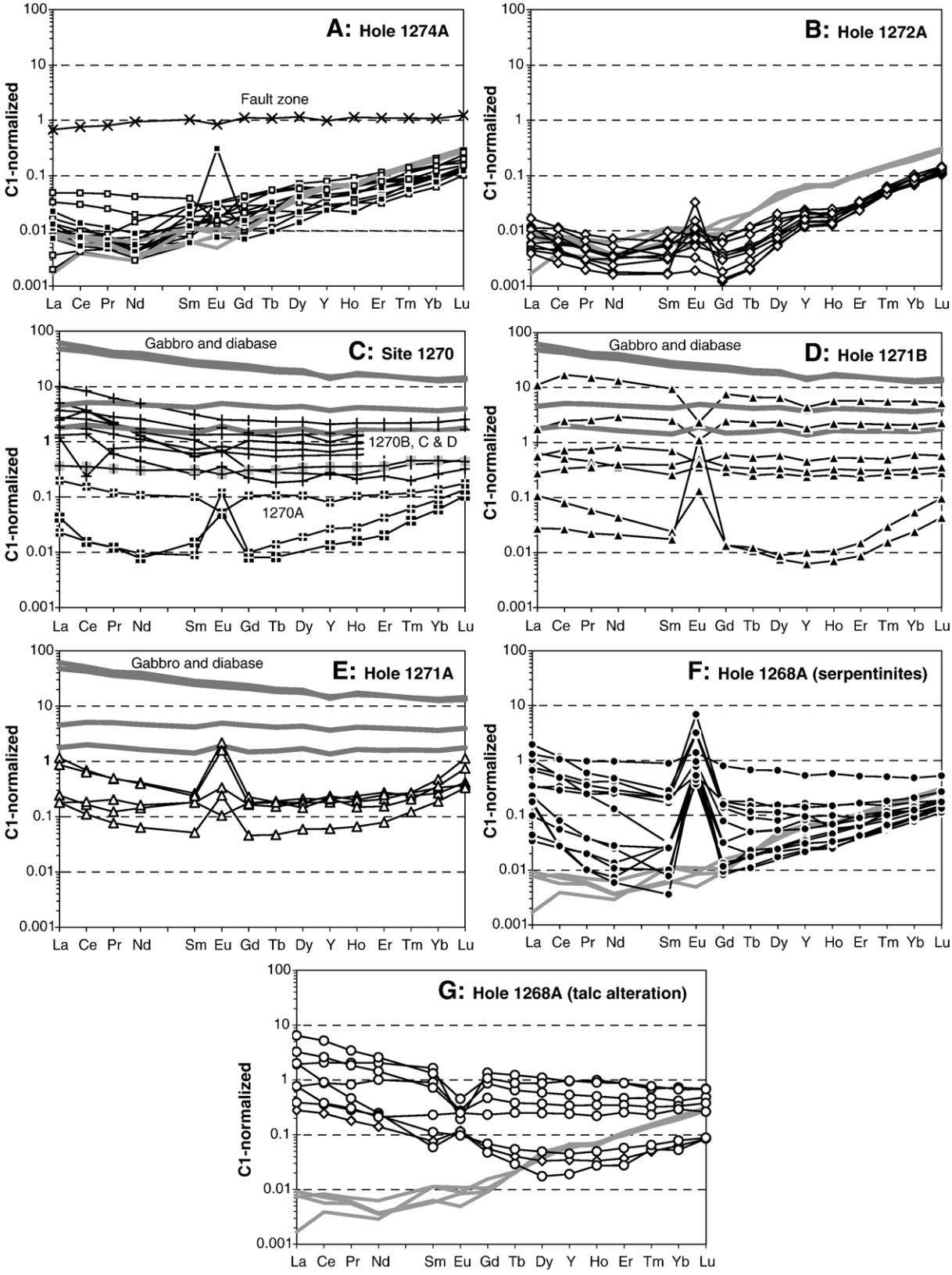
A: Hole 1274A
Fault zone
B: Hole 1272A
C: Site 1270
Gabbro and diabase
1270B, C & D
1270A
D: Hole 1271B
E: Hole 1271A
F: Hole 1268A (serpentinites)
G: Hole 1268A (talc alteration)
C1-normalized
100
10
1
0.1
0.01
0.001
La Ce Pr Nd Sm Eu Gd Tb Dy Y Ho Er Tm Yb Lu

et al., 2000; Godard et al., 2000; Bodinier and Godard, 2003; Niu, 2004).

In Hole 1274A, where the least-altered peridotites were sampled, the positive correlations of Al_2O_3 vs. V, Sc, and Cr can be linked to the variations in the modal proportions of pyroxene and olivine in the protolith since the dunites are more refractory in character than the associated harzburgite (Fig. 4A, B, C). Point counting results confirm that the modal proportion of pyroxene ($pyroxene_{modal}/[pyroxene_{modal}+olivine_{modal}]$) are correlated with the Al_2O_3 concentrations at this site (Fig. 4E). Since the data from the more intensely altered sites follow the same geochemical trends it can be inferred that Al, V, Sc, and Cr were immobile during hydrothermal processes. The peridotites from Hole 1274A also define linear arrays showing a small decrease in MgO and FeO_{total} and increase in SiO_2 with increasing Al_2O_3 (Fig. 4D, F, G). This is also consistent with the inferred relationship between modal pyroxene abundance and bulk rock geochemistry.

The most prominent effect of serpentinization is the addition of water to the rock and even the least-altered peridotites from Hole 1274A have H_2O contents of ~10 wt.% which increases to ~15 wt.% for complete serpentinization (Fig. 6A). Serpentinized dunites have even higher water contents (up to 17.5 wt.%) due to the formation of brucite. In terms of SiO_2 and MgO contents, most of the serpentinized peridotites cluster around the composition of serpentine, however, some brucite bearing dunites have MgO concentrations up to 50 wt.% (Fig. 6B). Another important effect of serpentinization is the change in Fe-oxidation state (Fig. 6D). The samples from Holes 1272A and 1274A cluster along a line defined by a constant Fe-budget where changes in FeO and Fe_2O_3 concentrations are attributable to the oxidation of ferrous iron in primary silicates to ferric iron in magnetite and/or serpentine. Data from Hole 1274A show that with progressive alteration the FeO concentrations decrease from 4 to 2 wt.% and the most Fe_2O_3-rich samples have the Fe_2O_3/FeO ratio of magnetite. This indicates that for completely serpentinized samples the Fe-budget is mainly controlled by the formation of magnetite.

The REE pattern of serpentinites form Holes 1272A and 1274A are largely similar to the least-altered samples except from some variability in LREE concentrations and the local development of a positive Eu-anomaly (Fig. 5A, B). Also, the concentrations of HREE at Site 1272 are consistently below the concentrations in least-altered samples from Site 1274 suggesting an even more depleted precursor composition or dilution of REE concentrations due to mass addition during serpentinization.

3.2. Sites 1270 and 1271

The composition of serpentinites from Sites 1270 and 1271 is generally similar to the serpentinites from Site 1274 and 1272 in terms of major element and most trace elements (Figs. 4 and 6). However, chromite is abundant at Site 1271 which is reflected in elevated Cr and FeO_{total} concentrations and lower SiO_2 contents (Figs. 4C, D, G; Shipboard Scientific Party, 2004).

Fig. 5. The REE-Y patterns of variably altered peridotite recovered from ODP Sites 1268, 1270, 1271, 1272, and 1274 are highly diverse reflecting primary characteristics, melt–rock interaction and effects of hydrothermal alteration (serpentinization and talc alteration). (A). The least-altered peridotite (heavy gray lines) from the upper 50 mbsf at Hole 1274A are strongly depleted in LREE, in keeping with the refractory character of common mid-ocean ridge mantle. Serpentinized harzburgite (white squares) and dunite (black squares) have similar LREE depleted pattern than least-altered peridotite. However, there is some variability in HREE and some samples appear to have gained LREE and Eu. A zone consisting of soft serpentine mud at 132 mbsf is interpreted as a fault zone (crosses) and shows a flat REE pattern at chondritic concentrations possibly due to localized melt–rock interaction processes. (B). The iowaite-bearing serpentinites from Hole 1272A are characterized by variable MREE and LREE concentrations and the development of positive Eu anomalies. The HREE contents are constant and lower compared to the least-altered peridotite from Hole 1274A (gray lines). (C). The smooth REE pattern of serpentinites from Holes 1270C and D (crosses) are flat to LREE enriched and show a remarkable similarity to mafic rocks sampled during ODP Leg 209. One sample of talc altered harzburgite from Hole 1270B shows the same characteristics (black cross on grey background). These features are consistent with petrographic characteristics indicating significant melt–rock interaction. In contrast, two samples from Hole 1270A (white cross on black background) show pronounced U-shaped pattern with strong positive Eu anomalies. These features are similar to the "fluid-dominated serpentinization" at Hole 1268A (F). (D). Similar to the samples from Holes 1270B, C, and D the REE data for most of the samples from Hole 1271B indicate interaction with a melt phase causing REE addition and flat to LREE enriched REE shapes. However, two samples from the upper 40 mbsf show U-shaped pattern with a strong positive Eu-anomaly similar to the "fluid-dominated serpentinization" at Hole 1268A (F). (E). The Hole 1271A was drilled immediately adjacent to Hole 1271B but reached only 40 mbsf. In this domain, the effects of melt–rock interaction processes appear to be less pronounced than further below in Hole 1271B. The REE pattern of Hole 1271A are strongly enriched in LREE compared to the least-altered peridotite sampled in Hole 1274A (A), however, most samples show U-shaped pattern and positive Eu anomalies. It is possible that melt–rock interaction and subsequent hydrothermal processes are both responsible for these characteristics.(F). Serpentinization at Hole 1268A generated peculiar U-shaped REE pattern with strong LREE enrichments and pronounced positive Eu anomalies. Whereas LREE and MREE show variations of about two orders of magnitude the HREE concentrations are remarkably constant. Heavy grey lines are least-altered peridotite from Hole 1274A. (G). Talc alteration at Hole 1268A that overprinted serpentinization, shows smooth, flat to LREE enriched pattern and most samples have a negative Eu-anomaly. Overall, REE concentrations are elevated compared to serpentinization. Heavy grey lines are least-altered peridotite from Hole 1274A.

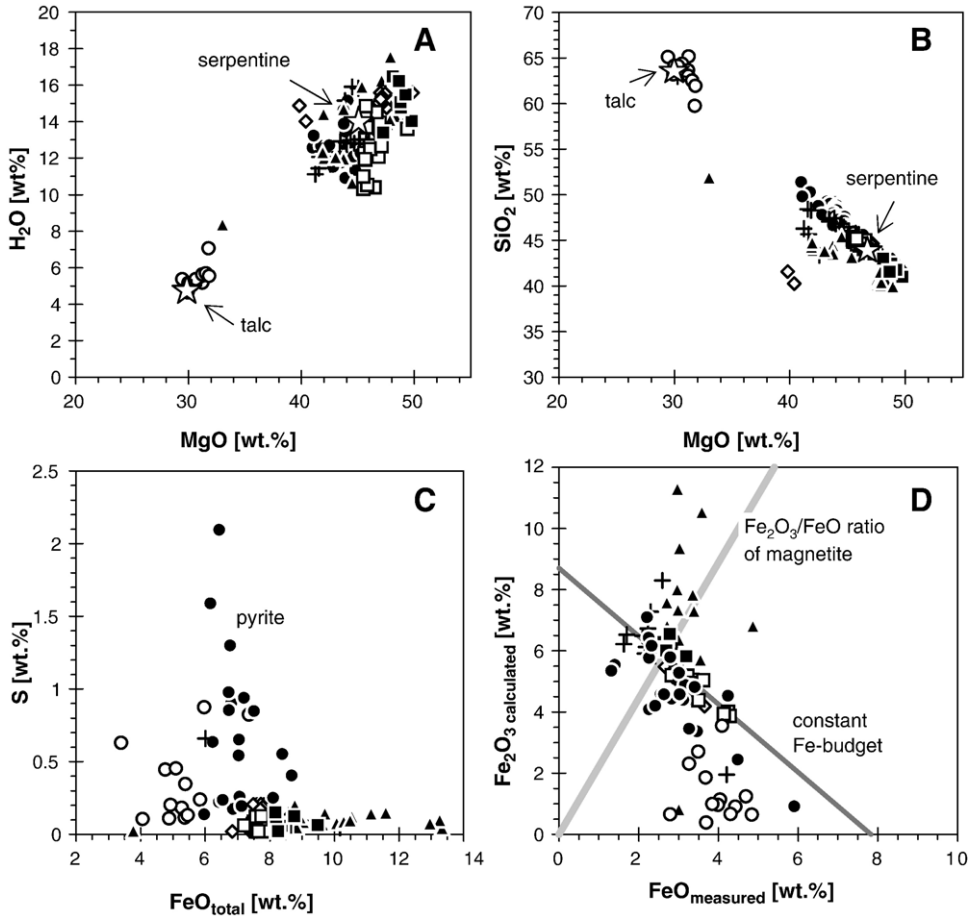

Fig. 6. In terms of major elements the effects of alteration are particularly apparent in variations of MgO, FeO_{total}, SiO_2, H_2O and S concentrations and the oxidation state of iron. Symbols as in Fig. 3. (A). MgO vs. H_2O (B). MgO vs. SiO_2 (C). FeO_{total} vs. S (D). $Fe_2O_{3\ calculated}$ vs. $FeO_{measured}$. Major element concentrations are recalculated to 100% anhydrous. The H_2O concentrations were measured directly on board the RV Joides-Resolution during ODP Leg 209 for 85 samples. For the remaining samples the H_2O contents have been calculated using the loss on ignition and the data for CO_2, S, and NO_3 (Supplementary Table).

The abundance of mafic dikelets and thin section scale melt impregnation textures in some drill holes of Sites 1270 and 1271 is reflected in particular REE systematics (Fig. 5C, D) and elevated concentrations of some incompatible elements (Zr, Th, U; Fig. 7). In contrast to the LREE depleted pattern of the peridotites from Holes 1274A and 1272A, samples from Holes 1270B, C, and D (Fig. 5C) and most samples from Hole 1271B (Fig. 5D) show flat to slightly LREE enriched pattern with chondrite-normalized concentrations ranging from 0.2 to 10. These are almost identical to analyses of mafic rocks sampled during ODP Leg 209 showing smooth, flat to LREE enriched pattern (Fig. 5C, D, E). Furthermore, peridotites from Holes 1270C and D and 4 samples from Hole 1271B have elevated U contents ranging from 0.4 to 1.4 ppm (Fig. 7A) and comparatively high concentrations of Th (0.02 to 0.46 ppm) and Zr (1 to 5 ppm, Fig. 7B). These characteristics suggest that the primary REE signatures and Th, U, and Zr concentrations of these peridotite samples, which probably had initial compositions similar to the refractory peridotite of Site 1274, were modified due to interaction with mafic to differentiated melts. Serpentinites from Holes 1270A, 1271A and two samples from Hole 1271B deviate from these characteristics introduced by melt–rock interaction processes. These samples show U-shaped REE patterns with positive Eu anomalies (Fig. 5C, D, E) that are either due to the addition of plagioclase during melt–rock interaction (e.g., Niu et al., 1997) or result from interactions with hydrothermal fluids similar to the serpentinites at Hole 1268A.

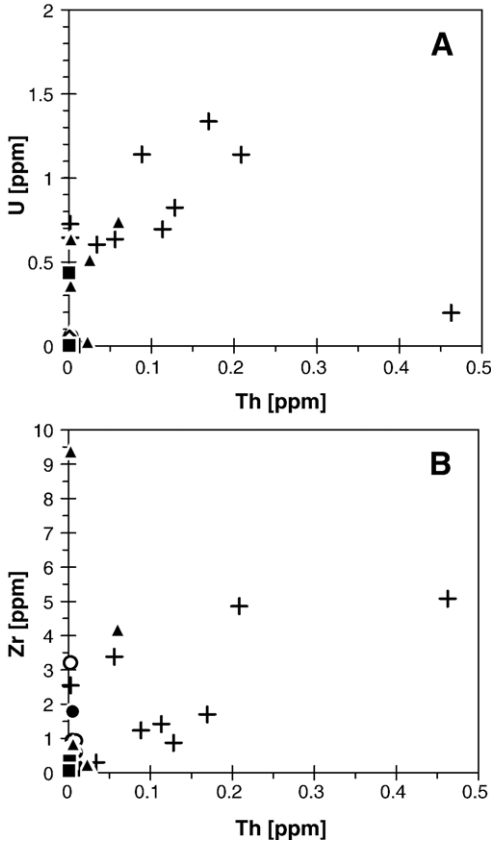

Fig. 7. Some serpentinites from Sites 1270 and 1271 show relatively high immobile trace element concentration indicative for melt–rock interaction processes. Symbols as in Fig. 3. (A). U vs. Th (B). Zr vs. Th.

3.3. Site 1268

The major and trace element concentrations of serpentinization at Hole 1268A are similar to the other serpentinites sampled during ODP Leg 209. However, the abundance of disseminated pyrite and pyrite veins is reflected in elevated S concentrations (range: 0.1 to 2.1 wt.%; average: 0.6 wt.%, Fig. 6C) and low Fe_2O_3/FeO ratios compared to serpentinites with magnetite as the principal Fe-hosting mineral phase. Remarkably, serpentinization at Hole 1268A is characterized by the development of strongly U-shaped REE patterns with pronounced positive Eu anomalies (Fig. 5F). The MREE and LREE show wide ranges of concentrations (variations of up to two orders of magnitude) whereas the HREE are comparatively constant (range of Lu_N: 0.11 to 0.27). The most extreme examples have positive LREE/HREE ratios and show distinct positive Eu anomalies.

Talc alteration at Hole 1268A supersedes serpentinization and is characterized by a decrease in H_2O (ranging mainly between 5 and 6 wt.% which corresponds to the water content of talc, Fig. 6A). Furthermore, talc altered rocks are SiO_2-rich (60 to 65 wt.%) with comparatively low MgO values (Fig. 6B) and characterized by higher FeO concentrations (4 to 5 wt.%) but considerably lower Fe_2O_3 concentrations (1 to 3 wt.%) than serpentinization. Also, the data plot below the line defining a constant Fe-budget (Fig. 6D) which may indicate that some Fe was lost or that the total Fe concentration was diluted due to a gain in SiO_2. This issue is further examined below (Discussion) using a mass balance approach. In contrast to serpentinization in Hole 1268A, the talc alteration is characterized by comparatively smooth, flat to LREE enriched patterns, and most samples show a well-developed negative Eu-anomaly (Fig. 5G).

4. Discussion

Recent studies have suggested that asthenospheric melting and refertilization by melt–rock interaction are the dominant processes controlling the major and trace element characteristics of abyssal peridotites (Niu et al., 1997; Niu, 2004). Our data show that this may only be true for fluid–peridotite interaction under certain conditions here referred to as rock-dominated serpentinization.

Fig. 8 summarizes the various processes affecting ascending refractory peridotite as evidenced in different locales sampled during ODP Leg 209. Melts rising through the lithosphere may interact with the peridotite and cause particular geochemical modifications (e.g., addition of SiO_2, REE and HFSE). In some instances, these melts may be channeled along ductile deformation zones that develop in response to tectonic strain. Evidence for such processes is preserved at Sites 1270 and 1271 where addition of mafic and differentiated melts imparted local enrichments in some trace elements (e.g., U, Th, Zr) and REE.

An initial stage of high-temperature (>375–400 °C) hydrothermal interaction of peridotite with hydrothermal solutions is documented by relict textures of orthopyroxene replacement by talc and tremolite at Sites 1270 and 1271 (Allen and Seyfried, 2003; Bach et al., 2004). This stage is overprinted by widespread serpentinization that may be largely isochemical (i.e., restricted to the addition of H_2O, rock-dominated serpentinization) or associated with particular geochemical modifications due to more intense interaction with hydrothermal fluids (fluid dominated serpentinization). Continued fluid–serpentinite interaction caused iowaite formation at Site 1272 (Bach et al., 2004) and serpentine replacement by talc at Site 1268.

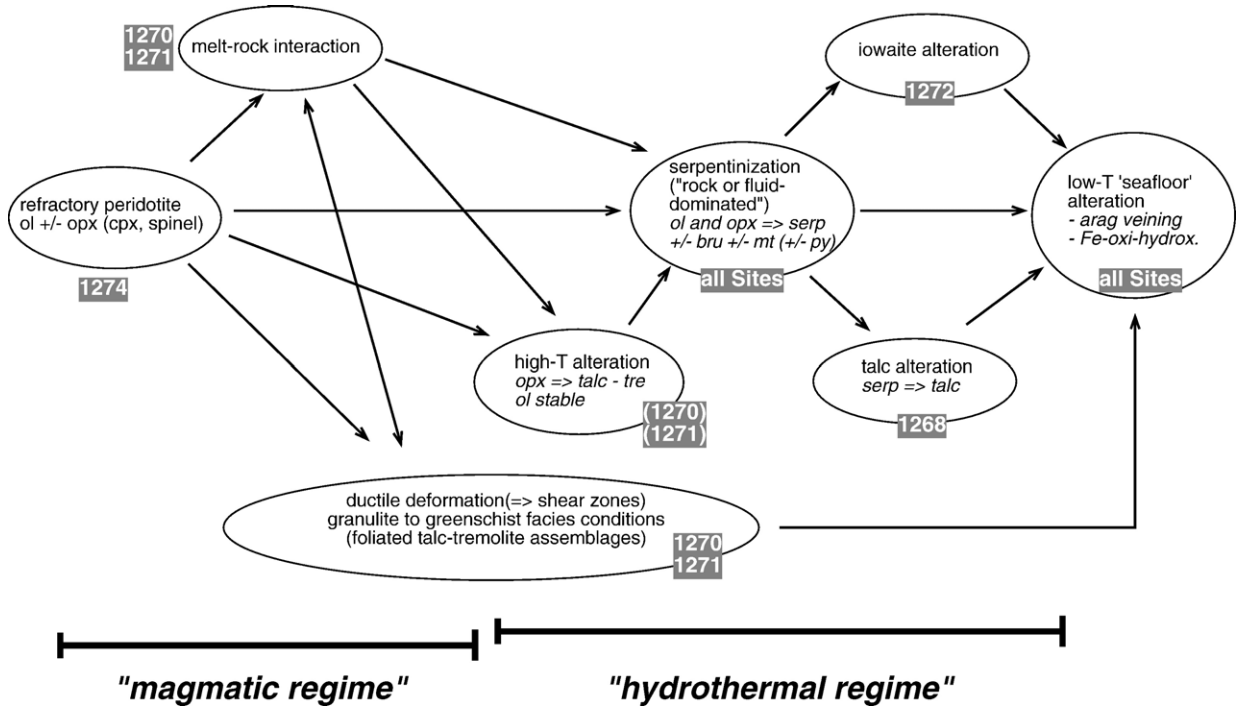

Fig. 8. Flow chart illustrating the processes affecting the composition of refractory peridotite within the thermal boundary layer and in the near-seafloor environment. The various pathways that are documented in the samples derived from ODP Leg 209 are indicated and the sites showing the relevant evidence are marked. A magmatic regime where ductile deformation and melt rock interaction processes are dominant is contrasted to a hydrothermal regime where temperatures are <450 °C and fluid–peridotite (and/or serpentinite) interaction causes the formation of various alteration assemblages.

The last stage of alteration is low-*T* interaction of the serpentinites with ambient seawater that circulates in the near seafloor environment, generating aragonite veinlets, Fe-oxyhydroxides, and clays.

The following discussion focuses on the geochemical processes in the "hydrothermal regime", excluding the high-*T* (replacement of orthopyroxene) and low-*T* (seafloor alteration) end-member conditions (Fig. 8). However, in order to assess element mobility under these hydrothermal conditions the influence of melt–rock interaction processes on the composition of Leg 209 peridotites needs to be considered first.

4.1. REE and HFSE systematics related to melt–rock interaction (Sites 1270 and 1271) and hydrothermal alteration (Sites 1274, 1272, and 1268)

The peridotites drilled during ODP Leg 209 show remarkable compositional variations and REE have been added during melt–rock interaction (Fig. 5C, D) and hydrothermal alteration (Fig. 5F, G). In order to investigate the relative importance of these processes at the different sites the behavior of HFSE and REE may be considered. In aqueous solutions, the LREE are more readily transported than HREE and HFSE whereas melt–rock interaction causes addition of LREE and HFSE to the rock in about equal proportions (Niu, 2004). In Fig. 9 the global abyssal peridotite data presented by Niu (2004) define positive trends in Nb vs. La and Th vs. Ce space which indicates that melt–rock interaction is the dominant factor controlling the compositional variation. However, the situation is considerably more complex in the 15°20′N area where two deviating trends can be observed. One trend is defined by the HFSE enriched samples that are mainly derived from Holes 1270B, C, and D and Hole 1271B. In line with the petrographic evidence for melt impregnation, these samples follow the trend of the global data set characterizing melt–rock interaction as the dominant process. A different trend is defined by data from Holes 1274A, 1272A and 1268A which show LREE enrichment correlated with only a minor increase in HFSE concentrations (Fig. 9A, B). This relationship indicates that LREE variability is largely due to hydrothermal alteration, which affects HFSE, like Th, to lesser extents. The most prominent example of hydrothermal alteration affecting REE contents (i.e., fluid-dominated alteration) are serpentinites and talc altered rocks from Hole 1268A.

In addition to the increase in LREE concentrations during magmatic and hydrothermal processes, increasing ratios of MREE/HREE (Gd_N/Lu_N) are apparent when samples from Sites 1268, 1270, and 1271 are compared to samples from Sites 1272 and 1274 (Fig. 5). These changes are correlated with high HFSE concentrations in many samples at Sites 1270 and 1271, whereas an array of increasing Gd_N/Lu_N at

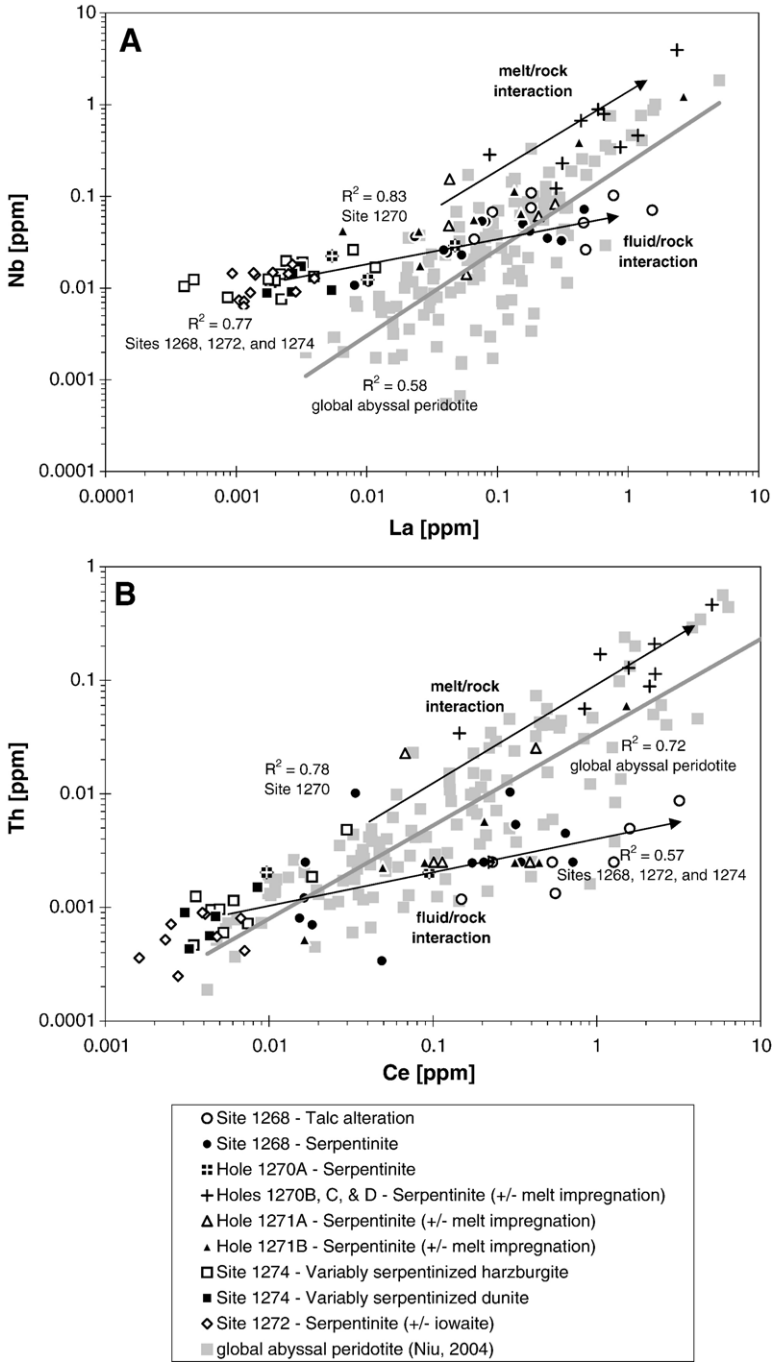

Fig. 9. Deviating trends for melt–rock interaction and hydrothermal alteration are defined in LREE vs. HFSE space. This is due to the higher solubility of LREE in aqueous solutions compared to HFSE. In contrast, LREE and HFSE are equally soluble in silicic melts. (A). Nb vs. La (B). Th vs. Ce (C). Nd vs. Gd_N/Lu_N (D). Th vs. Gd_N/Lu_N.

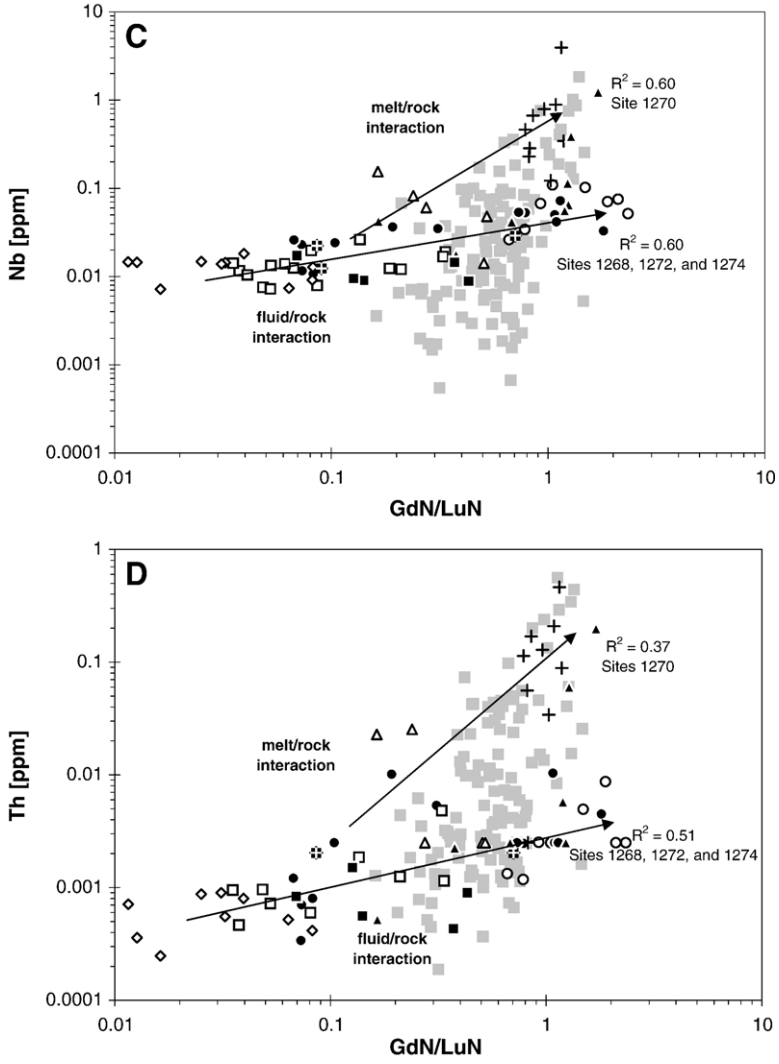

Fig. 9. (*continued*).

low HFSE concentrations is defined by data from Sites 1268, 1272, and 1274 (Fig. 9C, D). This is consistent with the interpretation that MREE have also been added locally by hydrothermal alteration. However, the relatively wide range of Gd_N/Lu_N ratios at Hole 1274A (rock-dominated serpentinization) suggest that primary variability in the peridotite protolith may also have played a role. It is important to note that some samples from Sites 1270 and 1271 do not follow the "melt–rock interaction trend" but show relatively low HFSE concentrations similar to the samples defining the "hydrothermal alteration trend". This may indicate that melt–rock interaction, and hence melt transport, was heterogeneous at the scale sampled by these drill holes.

4.2. Rock-dominated serpentinization: mass changes at Site 1274

The peridotite at Site 1274 shows successive replacement of olivine and pyroxene by serpentine± brucite±magnetite assemblages and serpentinization is complete below 60 mbsf (Fig. 2A). Nevertheless, it can be demonstrated that variations in the proportions of olivine and pyroxene in the protolith are responsible for the variations in Al_2O_3, SiO_2, MgO and FeO_{total} (Fig. 5). Hence, the relative proportions of these elements were preserved despite serpentinization indicating that they were immobile during fluid/rock interaction (cf. Niu, 2004). This interpretation is supported by microprobe data revealing distinctive compositions

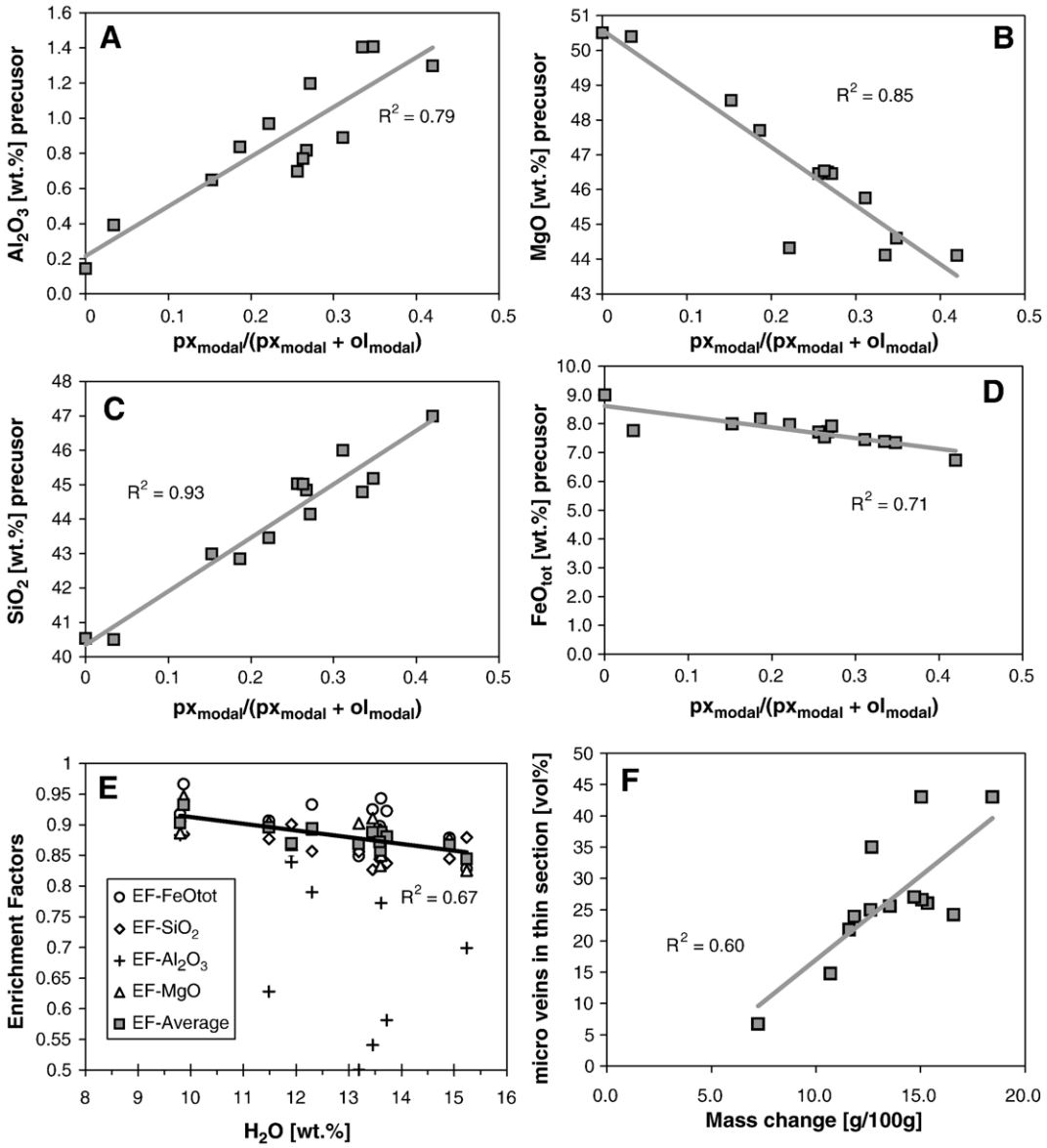

Fig. 10. Results of mass balance calculations for Hole 1274A. White squares: serpentinized harzburgite; black squares: serpentinized dunite. (A, B, C, and D). The reconstructed bulk rock geochemical composition of the precursor peridotites at Hole 1274A shows well constrained correlations with the modal proportions of pyroxene and olivine. This indicates that the recalculation process generated realistic results. (E). Enrichment factors have been calculated for each sample using SiO_2, Al_2O_3, MgO, and FeO_{total} as immobile monitor elements. The calculations based on SiO_2, MgO, and FeO_{total} yield consistent results and increasing H_2O contents of the samples are correlated with decreasing EF values. The EF values calculated based on the Al_2O_3 data show wide scatter. (F). There is a positive correlation among the calculated mass gains for the individual samples and the observed volume proportions of micro veins in thin sections. This indicates that the mass gain was accommodated by a volume increase during serpentinization.

for serpentine formed after orthopyroxene and serpentine formed after olivine (Moll et al., submitted for publication).

If serpentinization was isochemical and simply related to the addition of H_2O then an overall mass gain should cause a decrease in the measured concentrations of immobile elements in the serpentinized rocks compared to their unaltered precursor (Grant, 1986; MacLean, 1990; MacLean and Barrett, 1993; Barrett and MacLean, 1994). However, the samples from Hole 1274A are heterogeneous in their modal orthopyroxene to olivine ratios so that the precursor composition is distinctive for each sample. Hence, a precursor composition must be determined

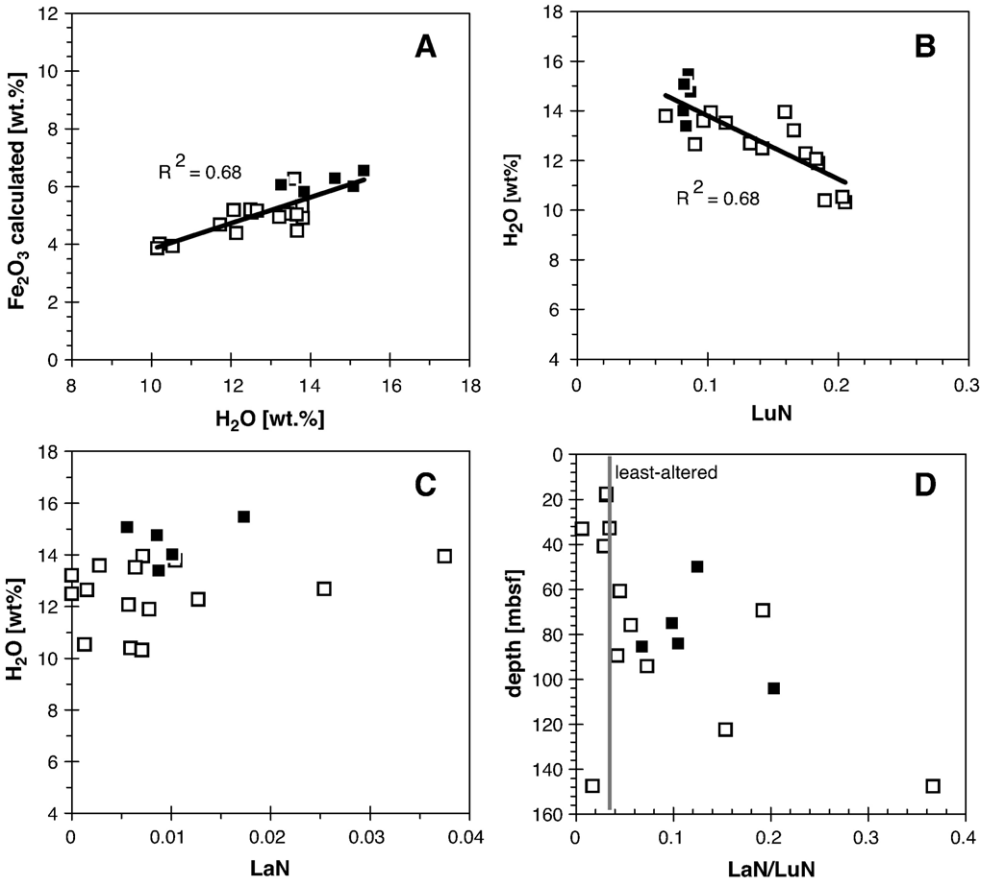

Fig. 11. Effects of hydrothermal alteration on Fe oxidation state and REE systematics at Hole 1274A. White squares: serpentinized harzburgite; black squares: serpentinized dunite. (A). A positive correlation of $Fe_2O_{3\ calculated}$ (determined from XRF analyses and FeO measurements using titration methods) and H_2O content demonstrates that increasing intensity of serpentinization is coupled with oxidation of iron. This is also reflected in the formation of magnetite at an advanced stage of serpentinization. (B). A negative trend of Lu_N and H_2O suggests that mass addition during serpentinization may have diluted the concentration of HREE which were immobile during hydrothermal alteration. However, it is difficult to ascertain that HREE concentrations were identical for all the samples prior to alteration and, hence, primary and secondary factors may both be important in generating this relationship. (C). Whereas a well-constrained trend exists for Lu_N and H_2O (B) the variations in La_N are not correlated with the degree of serpentinization. This suggests that La may have been mobile during alteration. Alternatively, it could be argued that La_N/Lu_N ratios were variable in the unaltered protoliths of Hole 1274A. (D). Elevated La_N/Lu_N ratios are common in the deeper portions of Hole 1274A where serpentinization is complete.

for each sample and compared to the measured composition of the altered rock in order to determine the elemental fluxes during alteration. It is possible to calculate these precursor compositions by combining the modal proportions of primary phases (determined from point counting) with the compositional data of these phases (microprobe analyses). In the case of Hole 1274A, trace amounts of fresh primary phases are preserved even in the most altered samples. The results of this procedure are presented in Table 4 (Appendix A).

As should be expected, the calculated composition of the precursor peridotites show well-constrained correlations for MgO, SiO_2, Al_2O_3, and FeO_{tot} concentrations with the modal proportions of pyroxene and olivine (Fig. 10A–D). The dunite and pyroxene-poor harzburgite ($pyroxene_{modal}/[pyroxene_{modal}+olivine_{modal}]<0.2$) have relatively low Al_2O_3 and SiO_2 concentrations but high MgO and FeO_{tot} values compared to the harzburgite with high modal pyroxene contents ($pyroxene_{modal}/[pyroxene_{modal}+olivine_{modal}]=0.3$ to 0.4). These correlations indicate that the data may be used to establish the mass changes during serpentinization at Hole 1274A.

In general, the budget of mass addition or loss during alteration can be quantified based on a comparison of the concentration of immobile elements in the precursor with that in the altered equivalent, since any differences

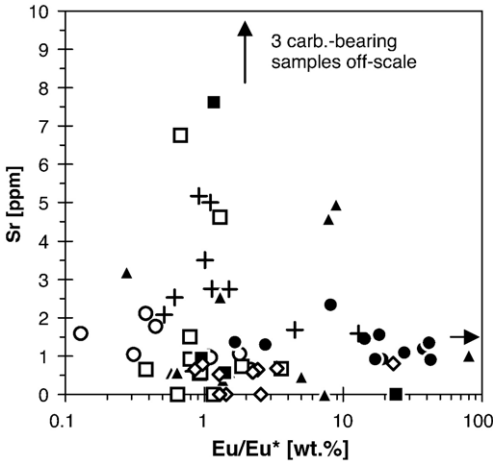

Fig. 12. Variations in the Eu/Eu∗ values show no correlation with Sr concentrations, hence, excluding the possibility that trace amounts of plagioclase could be responsible for the high Eu concentrations observed in samples representing fluid dominated serpentinization. Symbols as in Fig. 3.

must be caused by overall mass change. This relationship can be expressed as

$$c^{\text{precursor\_rock}}_{\text{immobile\_element}} \times \text{EF} = c^{\text{altered\_rock}}_{\text{immobile\_element}}$$

where c is the concentration and the enrichment factor (EF) is >1 if the rock lost mass during alteration and <1 if mass has been added. Assuming that only H_2O was added during serpentinization, SiO_2, MgO, FeO_{tot} and Al_2O_3 may be used to calculate EF values for the variably altered peridotite (Table 4). The results show that EF_{SiO_2}, EF_{MgO} and $EF_{FeO_{tot}}$ are within the range of 0.95 to 0.80 and values for each sample are narrowly constrained (Fig. 10E). Overall, there is a decrease in EF values with increasing H_2O content which supports the interpretation that H_2O addition to the rock during alteration was associated with successive mass gains. In contrast, the EF values calculated on the basis of Al_2O_3 concentrations show a large scatter and are generally lower than expected (Fig. 10E). This would suggest that Al_2O_3 was lost from the peridotite during serpentinization, which is unlikely given the low levels of Al in hydrothermal fluids venting from peridotite massifs (<3 μM; Douville et al., 2002). Alternatively, it may be inferred that the Al_2O_3 concentrations in the precursor have been overestimated. Since Al_2O_3 is concentrated in spinel, which is only a minor phase in the samples, an overestimation of its modal abundance during the point counting procedure has severe effects on the calculated concentrations in the precursor. Also, Al_2O_3 concentrations are mainly below 1 wt.% in the altered rocks, hence, there are profound effects on the EF value if the calculated concentration of Al_2O_3 precursor is overestimated by just 0.1 to 0.5 wt.%. Consequently, we consider the $EF_{Al_2O_3}$ values less reliable than the EF_{SiO_2}, EF_{MgO} and $EF_{FeO_{tot}}$ values.

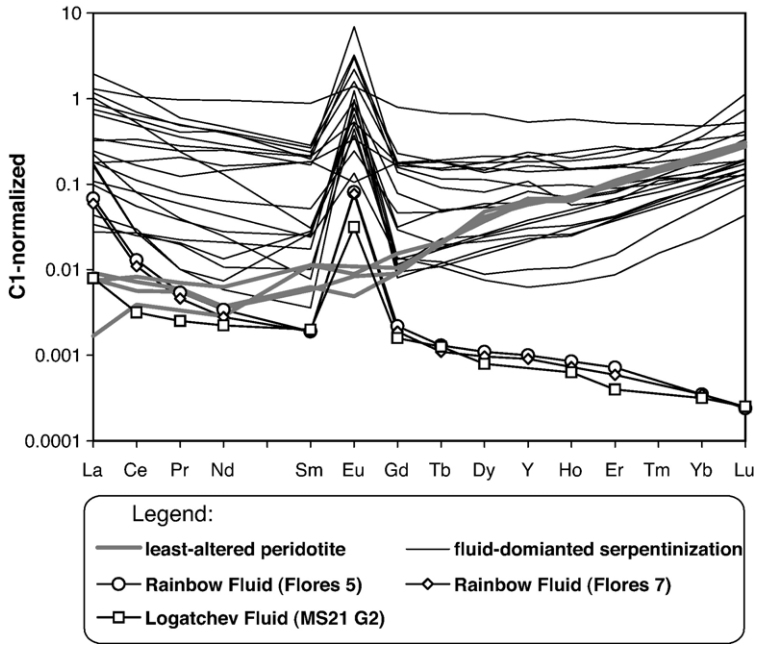

Fig. 13. Comparison of the REE pattern of serpentinites from Hole 1268A (fluid dominated serpentinization) with the composition of vent-type hydrothermal fluids sampled at the Rainbow and Logatchev ultramafic hosted hydrothermal systems. Fluid data from Douville et al., 1997 and 2002.

Table 5
Calculation of mass changes due to talc alteration of serpentinite at Hole 1268A

	Serpentinization (n=29)	Talc alteration (n=13)	constant mass	MgO immobile	SiO_2 immobile
	Average "precursor"	Average "altered rock"	Mass change [g/100 g]	Mass change [g/100 g]	Mass change [g/100 g]
SiO_2	41.74	59.77	18.03	36.84	0.00
MgO	38.14	29.01	−9.13	0.00	−17.88
H_2O	12.00	5.19	−6.81	−5.18	−8.38
FeO	1.75	3.43	1.68	2.76	0.65
Fe_2O_3	4.58	1.31	−3.27	−2.86	−3.67
FeS_2	0.97	0.54	−0.43	−0.26	−0.59
Total iron[a]	7.30	5.39	−1.91	−0.21	−3.54
TOTAL	99.71	99.74	0.03	31.42	−30.06

The EF_{MgO} is 1.315 and the EF_{SiO_2} is 0.698. For the constant mass scenario the EF is 1.
[a] Sum of FeO+Fe_2O_3+FeS_2. n=number of analyses. The geochemical data used for calculating the average compositions are documented in Table 4 and in Shipboard Scientific Party, 2004.

In order to determine the total mass change during alteration, the EF values calculated for each sample based on the SiO_2, MgO, and FeO_{total} concentrations have been averaged (Table 4; Fig. 10E). The relationship between mass change, measured and reconstructed concentrations and the calculated enrichment factor can be expressed as

$$\Delta X_{total} = (c_{total}^{altered\_rock}/EF_{average}) - c_{total}^{precursor\_rock}$$

where ΔX represent a mass change in [g/100 g]. The results show that mass addition was in the range of 10 to 20 g/100 g (Table 4, Fig. 10F) and a positive correlation of these mass changes with the volume of hydrothermal veins determined by point counting suggests that the additional mass was accommodated by volume expansion and hydrothermal veining (Fig. 10F).

These mass balance calculations support the interpretation that geochemical modifications of the peridotite in Hole 1274A were minimal and largely restricted to the addition of H_2O. However, whereas the content of total iron has not been affected by alteration, there is a considerable shift in oxidation state. The concentration of Fe_2O_3 is increasing from 4 to 6.5 wt.% with increasing H_2O values (Fig. 11A) which is consistent with the presence of magnetite in the more strongly altered samples.

4.3. Rock-dominated alteration: REE systematics at Sites 1274 and 1272

The least-altered peridotite and the completely serpentinized peridotite at Hole 1274A show generally similar LREE-depleted patterns which is consistent with the interpretation of quasi-isochemical serpentinization.

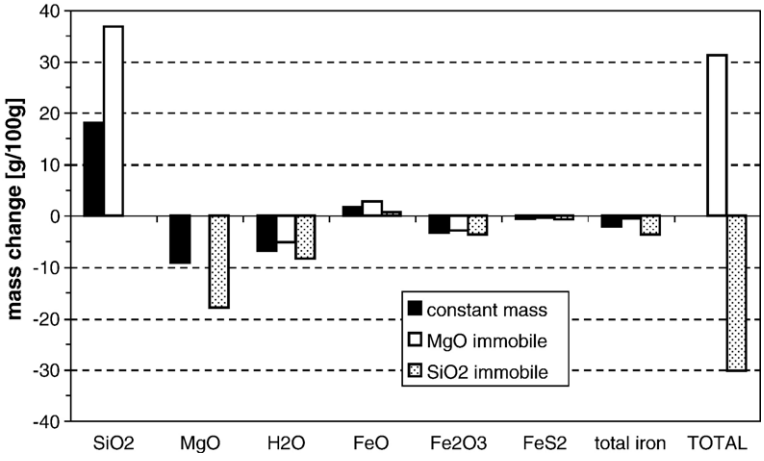

Fig. 14. Results of mass change calculations for talc alteration of serpentinite at Hole 1268A. Three different scenarios have been considered: no mass change, immobility of SiO_2 and immobility of MgO. Based on textural observations and considerations regarding reaction processes (Bach et al., 2004) it is inferred that immobility of MgO is the most likely scenario. Mass addition of SiO_2 is at least partially accommodated by hydrothermal veining and volume expansion. Data are presented in Tables 4 and 5.

However, there are variations in the HREE contents and the LREE/HREE ratios, and some samples show positive Eu anomalies. At Hole 1272A, the serpentinites show narrowly constrained Lu_N values below the concentrations in the least-altered peridotite. The LREE and MREE are somewhat variable and positive Eu anomalies are common.

Potentially, all these variations may be attributable to slight differences in the primary mineral assemblages. The principal carrier of the REE signature in these peridotites is clinopyroxene, which may vary in abundance and composition, and the development of a positive Eu-anomaly could be due to the presence of plagioclase, potentially introduced by melt–rock interaction. However, there is evidence indicating that hydrothermal processes are also important, in particular, for the development of Eu anomalies.

With regard to the HREE concentrations it may be inferred that primary composition and hydrothermal alteration both contribute to the well-constrained trend of decreasing Lu_N concentrations with increasing degree of serpentinization reflected in H_2O concentrations (Fig. 11B). In dunite the high modal proportion of olivine favors the formation of serpentine–brucite assemblages causing high H_2O concentrations during alteration and the scarcity of ortho- and clinopyroxene in the protolith could be responsible for low Lu concentrations in the precursor. Hence, the low Lu_N concentrations (Fig. 11B) are probably due to the primary modal characteristics and dilution related to mass gain during serpentinization. However, there is no correlation between La_N and H_2O (Fig. 11C), which could be explained by invoking La mobility during serpentinization if a constant La_N/Lu_N ratio in the unaltered precursors of the Hole 1274A samples is assumed. Elevated La_N/Lu_N values are particularly common in the lower portion of the drill hole where intense faulting has been observed (Fig. 11D) which may have facilitated serpentinization in this area by providing fluid pathways. Nevertheless, similar relative enrichments observed in highly refractory peridotites have been previously attributed to late melt/rock interaction associated with melt extraction and transport (e.g., Navon and Stolper, 1987; Godard et al., 1995). In fact, minor differences in the abundance and composition of clinopyroxene may readily explain the variations of Lu_N/La_N ratios at Hole 1274A.

Several samples from Holes 1274A and 1272A show a positive Eu-anomaly (Fig. 5A and B) which could be an indication for the former presence of plagioclase. There are three samples from Hole 1274A showing elevated Sr concentrations (4 to 8 ppm, Fig. 12) which could be supporting evidence for such a conclusion. However, all the samples from Hole 1272A have Sr concentrations <1.5 ppm and serpentinites from Hole 1268A, where serpentinization is characterized by strongly positive Eu anomalies, are also Sr poor. Also, no relicts of plagioclase were observed in thin sections. In addition, there is no correlation between Eu/Eu* and Sr and therefore relict plagioclase is probably not important in controlling the Eu-systematics for most samples. Consequently, it seems more likely that interaction with hydrothermal fluids during serpentinization resulted in local addition of Eu. This suggests that the serpentinizing fluid leached Eu during fluid–rock interaction prior to reacting with the sampled peridotites. Eu mobility is much increased compared to that of the trivalent REE under highly reducing conditions and high Cl-contents (Allen and Seyfried, 2005). The positive Eu-anomaly may therefore have been imposed during serpentinization in Holes 1274A and 1272A, even though alteration was largely rock dominated.

4.4. Fluid-dominated serpentinization: Site 1268

The serpentinites showing S addition (Hole 1268A; Fig. 7C) and U-shaped REE patterns with strong positive Eu anomalies (Hole 1268A and some serpentinites of Sites 1270 and 1271; Fig. 5) are interpreted to have experienced fluid-dominated serpentinization. It is unlikely that the positive Eu-anomaly can be attributed to relict plagioclase since Sr concentrations are below 2 ppm for most samples (Fig. 12).

The REE patterns of the Hole 1268A serpentinites deviate strongly from the least-altered peridotites but show similarities to the REE characteristics of hydrothermal fluids discharging at black smokers of ultramafic-hosted systems at the seafloor, such as the Rainbow and Logatchev hydrothermal sites (Fig. 13). End member compositions of these hot (350 to 400 °C) metal and S-rich fluids are characterized by positive La_N/Lu_N ratios and strong positive Eu anomalies (Douville et al., 1997, 2002). It has been suggested that these REE characteristics are due to equilibration with plagioclase-bearing lithologies during circulation within the oceanic crust (Klinkhammer et al., 1994; Douville et al., 2002). However, recent experimental studies demonstrate that the chlorinity and redox potential of the fluid is a major controlling factor on LREE and Eu complexiation and transportation (Allen and Seyfried, 2005) and that the presence of plagioclase is not required for the generation of LREE enriched fluid compositions with positive Eu anomalies.

Apparently, interaction of refractory peridotite with a hot, black smoker type hydrothermal fluid will strongly

influence the REE systematics of the resulting serpentinite, given sufficient fluid/rock ratios. Clearly, the LREE and Eu are likely to be affected most strongly since HREE concentrations in the fluids are 3 to 4 orders of magnitude lower than in the peridotite (Fig. 13). This may explain why the HREE of serpentinites at Hole 1268A are fairly constant whereas LREE and MREE are highly variable (Fig. 5F). Interaction with black smoker type hydrothermal fluids may generate successively more modified REE pattern in the serpentinites and the samples with highest La_N/Lu_N and Gd_N/Lu_N ratios probably represent the most mature stage of this process.

These considerations imply that LREE and MREE were incorporated in the rock during serpentinization. However, it is difficult envisage that the LREE and MREE were preferentially incorporated in serpentine minerals since the effective atomic radius of HREE are comparable to Mg (0.89) whereas LREE are similar to Ca (1.12; octahedral coordination; Shannon, 1976). Either the fluid/rock ratio was so high that the REE content of serpentine was entirely controlled by the fluid or there may be trace amounts of hydrothermal REE-bearing phases imparting the particular characteristics onto the rocks. This issue could be addressed by in-situ analytical techniques (LA-ICP-MS) and investigations regarding the microscale variations in the REE systematics of the serpentinites. In any case, high fluid fluxes are required to add sufficient amounts of REEs to the rock in order to erase the LREE depleted character of the protolith. Hence, based on the available data, it can be concluded that the time-averaged signal of serpentinization involving vent-type hydrothermal fluids imparts a particular; LREE and Eu enriched REE pattern on the rock and this style of alteration is referred to as fluid-dominated serpentinization.

4.5. Talc alteration: Site 1268

Talc alteration at Site1268 overprinted serpentinization and clearly modified the bulk rock compositions in terms of the Mg/Si ratios, H_2O contents, and REE systematics. Quantification of the geochemical budget of this process is difficult since both the composition of the serpentinites and the talc alteration in Hole 1268A show significant variability that can be attributed to differences in the modal composition of the protoliths. This is particularly evident for Al_2O_3 concentrations which range from 0.1 to 1.2 wt.% for both serpentinization and talc alteration suggesting substantial primary variability of the precursor peridotite in terms of the concentration of spinel and the modal proportions of pyroxene and olivine (Fig. 4). However, in order to gain a first order approximation of the general trends in the mass budget of the major components (SiO_2, Al_2O_3, FeO, Fe_2O_3, FeS_2, MgO, H_2O) the average composition of the serpentinites may be compared to the average composition of the talc alteration. For this exercise three different scenarios have been considered: 1) talc alteration of serpentinization took place without mass change, 2) MgO was immobile during alteration, and 3) SiO_2 was immobile (Table 5; Fig. 14).

Assuming that no mass change took place during talc alteration (EF = 1) the ΔX can be calculated by simple subtraction of the concentration of the component in the altered rock (talc alteration) from the concentration in the precursor (serpentinization). In this model, the rock would have gained SiO_2 (18 g/100 g) and lost H_2O, MgO and total iron (mainly in the form of Fe_2O_3 and FeS_2). An alternative scenario is provident by the assumption that MgO remained immobile during talc alteration (EF = 1.315). Due to the higher Si/Mg ratio of talc compared to serpentine this calculation results in a large mass gain of SiO_2 (37 g/100 g). This is partially offset by loss of H_2O (−5 g/100 g), however, the calculated total mass gain is substantial (31 g/100 g). Interestingly, the iron budget is almost neutral and gains in FeO are offset by the loss in Fe_2O_3. Hence, iron may have remained largely immobile during talc alteration and the calculated mass changes for the different iron species reflect adjustments to the new physico-chemical conditions. This model is supported by considerations regarding the fluid chemistry of talc alteration which indicate that Si-rich and Mg-saturated fluids are responsible for the replacement of the serpentine (Bach et al., 2004). However, the high total mass gain calculated for this process invokes substantial volume expansion. Assuming a simple reaction of 1 $Mg_3Si_2O_5(OH)_4$ (serpentine) + 2 $SiO_{2,aq}$ = 1 $Mg_3Si_4O_{10}(OH)_2$ (talc) + H_2O a volume increase of 27% can be calculated based on the molar volumes of talc (140 cm^3/mol) and chrysotile (110 cm^3/mol; Robie et al., 1979). In this regard, it is important to consider the relatively high abundance of hydrothermal veins estimated from core logging data at Hole 1268A (Table 1, Shipboard Scientific Party, 2004; Bach et al., 2004). Here, 8.9% of the drill core consist of macroscopic hydrothermal veins and about half of these are filled by talc. Potentially, the mass addition associated with Si metasomatism during talc alteration of serpentinite is accommodated by volume expansion and associated veining.

An additional calculation is based on the assumption that SiO_2 was immobile during the replacement of serpentinite by talc (EF = 0.698; Fig. 14). In this case, high losses in all other major components are required in

order to modify the elemental proportions appropriately resulting in a total mass loss of − 30 g/100 g. In particular, substantial MgO would need to be removed from the rock (− 18 g/100 g) which appears to be an unlikely scenario since the solubility of hydrous Mg-silicates in hydrothermal fluids is extremely low (e.g., Saccocia et al., 1994).

Overall, it may be concluded that talc alteration of serpentinites at Hole 1268A was associated with large total mass gains due to SiO_2 addition from a high a_{SiO_2} fluid which may have been accommodated by volume expansion associated with intense hydrothermal veining. The high a_{SiO_2} fluids may have been derived from pyroxene destructive alteration of peridotite or gabbro at depth (Bach et al., 2004). Similarly, interactions with gabbro may well be the source of sulfides in rocks from Hole 1268A, as suggested by Alt and Shanks (2003) for sulfides in serpentinites from the 23°N area on the Mid-Atlantic Ridge. Alternatively, fluids with high sulfur fugacities could be produced during desulfurization of primary sulfides at a serpentinization front deep in the system.

The REE signature of talc alteration deviates substantially from the characteristics of serpentinization at Hole 1268A (Fig. 4). Serpentinization is characterized by U-shaped patterns with strong positive Eu anomalies, whereas the talc alteration results in negative Eu anomalies and gently sloping or flat patterns. Also, the overall concentrations of REE increased despite mass addition to the serpentinites, which would have the tendency to dilute the concentration of any element considered to be immobile, such as the HREE. Apparently, LREE, MREE, and HREE have been added during talc alteration in particular proportions generating comparatively smooth patterns. However, Eu does not adhere to this trend and Eu/Eu* values are generally <1.

It is difficult to conclude how the particular REE signature of talc alteration was generated. Maybe Eu resided in a different phase than the other REE in the serpentinite protolith. Upon talc alteration, the Eu-bearing phase may have been destroyed while the other REE-bearing phase is stable. Alternatively, it may be possible that REE, including Eu, are all substituted into the serpentine structure and that recrystallization released Eu because it does not fit into the crystal lattice of talc. However, talc rocks with prominent positive Eu anomalies are known from submarine hydrothermal breccias and hydrothermally altered gabbroic rocks (D'Orazio et al., 2004).

Boschi et al. (2006) observed considerable REE and HFSE variations and variable Eu anomalies in schistous talc- and amphibole-rich metasomatized ultramafic rocks from Atlantis Massif and concluded that these might be due to fluid rock interactions, although melt impregnation processes cannot be ruled out. While hydrothermal mobilization of REE and HFSE seems plausible in schistous rocks from detachment faults that focused fluid flow, such mass transfers are more difficult to envision in situations of static alteration such as recorded in Hole 1268A. It is possible, however, that the talc alteration in Hole 1268A took place immediately adjacent to shear zones as suggested by Boschi et al. (2006) for static metasomatisms at Atlantis Massif. In that instance, the variability in REE contents in rocks from Hole 1268A may reflect different degrees of infiltration by synkinematic metasomatic fluids that migrated along a detachment fault.

5. Conclusions

The mantle section drilled in the 15°20′N area shows that there are considerable compositional heterogeneities within a MAR segment of less than 100 km in length due to magmatic and hydrothermal processes. Overall, the peridotites are depleted in several incompatible elements (e.g., Al, Sc, V) indicating a refractory starting composition.

At Sites 1270 and 1271, melt–rock interaction processes are prevalent generating smooth, LREE enriched pattern similar to the pattern of gabbroic rocks. Here, the elevated LREE concentrations and LREE/HREE ratios are correlated with increasing HFSE contents indicating that both were introduced by a melt phase. In contrast, samples of altered peridotite from Sites 1274, 1272, and 1268 define different trends where increasing LREE concentrations correlate with only slightly increasing HFSE contents. Since the solubility of LREE in aqueous solutions is higher than the solubility of HFSE it is inferred that this trend is due to hydrothermal alteration processes.

Serpentinization took place under variable conditions which can be described as "rock-dominated" and "fluid-dominated". Fluid-dominated serpentinization at Hole 1268A is characterized by addition of S, dominantly in the form of pyrite, and the formation of U-shaped REE pattern with strong positive Eu anomalies. These REE pattern are similar to the REE characteristics of hot (350 to 400 °C) hydrothermal fluids discharging at black smoker sites of ultramafic hosted hydrothermal systems such as Rainbow and Logatchev. Hence, it is inferred that serpentinization involving vent-type fluids and high fluid/rock ratios imposed the REE signature of the fluid onto the serpentinites.

Rock-dominated serpentinization at Sites 1274 and 1272 is characterized by little geochemical deviation

from the precursor compositions except for the addition of H_2O causing an overall mass gain of up to 20 g/100 g. The REE patterns are essentially similar to the least-altered peridotite sampled at the upper portion of Hole 1274A. Some of the variability in LREE concentrations could be related to hydrothermal alteration and/or localized melt/rock interaction. The presence of some samples with positive Eu anomalies is most likely caused by addition of Eu during fluid/rock interaction.

Talc alteration under static conditions of serpentinites at Hole 1268A was due to interaction with high a_{SiO_2} fluids and associated with substantial mass addition (in the order of 30 g/100 g). Furthermore, REE are apparently added to the rock generating smooth REE patterns, however, strong negative Eu anomalies are prevalent.

Overall, it can be concluded that hydrothermal processes are capable of locally generating a wide spectrum of REE patterns controlled by variations in alteration conditions. The evolution of the REE characteristics can be envisioned as a continuum from LREE depleted (Holes 1274A and 1272A) to hydrothermal vent fluid type patterns (serpentinites at Hole 1268A) on to LREE and MREE enriched patterns (talc alteration at Hole 1268A). These findings have important bearings on the interpretation of REE data from completely serpentinized abyssal peridotite. Clearly, variations in LREE alone are unreliable as indicators for the nature of the mantle protolith or the melt–rock interaction processes. Also, the budget of geochemical exchange processes between the hydrosphere and lithosphere at ultraslow spreading ocean ridges need to take into account that serpentinites may represent an important sink for Eu and LREE under fluid-dominated alteration conditions. However, it should be emphasized that the precise mechanism of the incorporation of REE in serpentinites is poorly understood. It needs to be established whether the REE are hosted within the serpentine minerals or whether there are accessory phases present that control the REE systematics. Such research would require the application of in-situ analyses such as LA-ICP-MS and may also elucidate the controls on the development of the particular REE pattern associated with talc alteration.

Acknowledgements

The authors would like to acknowledge the tremendous efforts of the entire crew of the “Joides-Resolution” during Ocean Drilling Program Leg 209. Melanie Moll, Beate Spiering, and Radegund Hoffbauer assisted with microprobe analyses and XRF measurements at the University of Bonn. We thank M. Rosner and J. Erzinger (GFZ Potsdam) for providing FeO, CO_2, H_2O, and S analyses. Funding was provided by the German Research Foundation (DFG) to HP. This research used data and samples supplied by the Ocean Drilling Program (ODP). ODP is sponsored by the U.S. National Science Foundation (NSF) and participating countries under management of Joint Oceanographic Institutions (JOI), Inc. **[RLR]**

Appendix A. Supplementary data

Supplementary data associated with this article can be found, in the online version, at doi:10.1016/j.chemgeo.2006.04.011.

References

Allen, D.E., Seyfried, W.E., 2003. Compositional controls on vent fluids from ultramafic hosted hydrothermal systems at mid-ocean ridges: An experimental study at 400 degrees C, 500 bars. Geochim. Cosmochim. Acta 67, 1531–1542.

Allen, D.E., Seyfried, W.E., 2005. REE controls in ultramafic hosted mid-ocean ridge hydrothermal systems: an experimental study at elevated temperature and pressure. Geochim. Cosmochim. Acta 69, 675–683.

Alt, J.C., Shanks III, W.C., 1998. Sulfur in serpentinized oceanic peridotites: serpentinization processes and microbial sulfate reduction. J. Geophys. Res. 103, 9917–9929.

Alt, J.C., Shanks III, W.C., 2003. Serpentinization of abyssal peridotites from the MARK area, 814 mid-atlantic ridge: sulfur geochemistry and reaction modeling. Geochim. Cosmochim. Acta 67, 641–653.

Bach, W., Paulick, H., 2004. C and O isotope composition of carbonates from serpentinites at the mid-Atlantic Ridge 14–16°N, Ocean Drilling Program Leg 209. European Geoscience Union. Geophysical Research Abstracts, Nice, EGU04-A-05790.

Bach, W., Banerjee, N.R., Dick, H.J.B., Baker, E.T., 2002. Discovery of ancient and active hydrothermal systems along the ultra-slow spreading Southwest Indian Ridge 10°–16°E. Geochem., Geophys., Geosys. 3, 279–289.

Bach, W., Garrido, C.J., Paulick, H., Harvey, J., Rosner, M., 2004. Seawater–peridotite interactions: first insights from ODP Leg 209, MAR 15°N. Geochem., Geophys., Geosys. 5, doi:10.1029/2004GC000744.

Barrett, T.J., MacLean, W.H., 1994. Mass changes in hydrothermal alteration zones associated with VMS deposits of the Noranda area. Explor. Min. Geol. 3, 131–160.

Batuev, B.N., Krotov, A.G., Markov, V.F., Cherkashov, G.A., Krasnov, S., Lisitsin, Y.D., 1994. Massive sulfide deposits discovered and sampled at 14°45′N, Mid-Atlantic Ridge. BRIDGE Newsl. 6, 6–10.

Bodinier, J.-L., Godard, M., 2003. Orogenic, ophiolitic, and abyssal peridotites. In: Holland, N.D., Turekian, K.K. (Eds.), Treatise on Geochemistry Volume 2: The mantle and core. Elsevier, Amsterdam, pp. 103–170.

Bogdanov, Y.A., Bortnikov, N.S., Vikentyev, I.V., Gurvich, E.G., Sagalevich, A.M., 1997. A new type of modern mineral-forming system: black smokers of the hydrothermal field at 14°45′ N Latitude, Mid-Atlantic Ridge. Geol. Ore Depos. 39, 58–78.

Boschi, C., Früh-Green, G.L., Delacour, A., Karson, J.A, Kelley, D. S., 2006. Mass transfer and fluid flow during detachment faulting and development of an oceanic core complex, Atlantis Massif (MAR 30°N). Geophys., Geochem., Geosys. 7, doi:10.1029/2005GC001074.

Charlou, J.L., Bougault, H., Appriou, P., Nelsen, T., Rona, P.A., 1993. Different TDM/CH_4 hydrothermal plume signatures: TAG site at 26°N and serpentinized ultrabasic diapir at 15°05′N on the Mid-Atlantic Ridge. Geochim. Cosmochim. Acta 55, 3209–3222.

Charlou, J.L., Fouquet, Y., Bougault, H., Donval, J.P., Etoubleau, J., Baptiste, J.P., Arnaud, D., Appriou, P., Rona, P.A., 1998. Intense CH_4 plumes generated by serpentinization of ultramafic rocks at the intersection of the 15°20′N fracture zone and the Mid-Atlantic Ridge. Geochim. Cosmochim. Acta 62, 2323–2333.

Cochran, J.R., Kurras, G.J., Edwards, M.H., Coakley, B.J., 2003. The Gakkel Ridge; bathymetry, gravity anomalies and crustal accretion at extremely slow spreading rates. J. Geophys. Res. 108 (B2), doi:10.1029/2002JB001830.

Dick, H.J.B., Lin, J., Schouten, H., 2003. An ultraslow-spreading class of ocean ridge. Nature 426, 405–412.

Douville, E., Charlou, J.L., Donval, J.P., Radford-Knoery, J., Fouquet, Y., Bienvenu, P., Appriou, P., Flores Cruise Scientific Party, 1997. Trace elements in fluids from the Rainbow hydrothermal field (36°14′N, MAR): a comparison with other Mid-Atlantic Ridge fluids. Eos Trans. 78, 832 (abstract).

Douville, E., Charlou, J.L., Oelkers, E.H., Bienvenu, P., Jove Colon, C.F., Donval, J.P., Fouquet, Y., Pricur, D., Appriou, P., 2002. The Rainbow vent fluids (36°14′N, MAR): The influence of ultramafic rocks and phase separation on trace element content in mid-atlantic ridge hydrothermal fluids. Chem. Geol. 184, 37–48.

D'Orazio, M., Boschi, C., Brunelli, D., 2004. Talc-rich hydrothermal rocks from the St. Paul and Conrad fracture zones in the Atlantic Ocean. Eur. J. Mineral. 16, 73–83.

Edmonds, H.N., Michael, P.J., Baker, E.T., Connelly, D.P., Snow, J., Langmuir, C.H., Dick, H.J.B., Mühe, R., German, C.R., Graham, D.W., 2003. Discovery of abundant hydrothermal venting on the ultra-slow spreading Gakkel ridge in the Arctic Ocean. Nature 421, 252–256.

Escartín, J., Hirth, G., Evans, B., 1997. Effects of serpentinization on the lithospheric strength and the style of normal faulting at slow-spreading ridges. Earth Planet. Sci. Lett. 151, 181–189.

Escartín, J., Mével, C., Macleod, C.J., McCraig, A.M., 2003. Constraints on deformation conditions and the origin of oceanic detachments, the Mid-Atlantic Ridge core complex at 15°45′N. Geochem., Geophys., Geosys. 4, doi:10.1029/2002GC000472.

Früh-Green, G.L., Kelley, D.S., Bernasconi, S.M., Karson, J.A., Ludwig, K.A., Butterfield, D.A., Boschi, C., Proskurowski, G., 2003. 30,000 years of hydrothermal activity at the Lost City Vent Field. Science 301, 495–498.

Früh-Green, G.L., Connolly, J.A.D, Kelley, D.S., Plas, A., Grobéty, B., 2004. Serpentinization of oceanic peridotites: implications for geochemical cycles and biological activity. In: Wilcock, W.D., Kelley, D.S., DeLong, E., Cary, C. (Eds.), The sub seafloor biosphere at Mid-Ocean Ridges. AGU Geophysical Monograph, vol. 144, pp. 119–136.

German, C.R., Baker, E.T., Mével, C., Tamaki, K., et al., 1998. Hydrothermal activity along the southwest Indian ridge. Nature 395, 490–493.

Gibson, I.L., Beslier, M.O., Cornen, G., Milliken, K.L., Seifert, K.E., 1996. Major-and trace element seawater alteration profiles in serpentinite formed during the development of the Iberian margin, Site 897. In: Whitmarsh, R.B., Sawyer, D.S., Klaus, A., Masson, D.G. (Eds.), Proc. ODP, Sci. Repts., vol. 149. Ocean Drilling Program, College Station TX, pp. 519–527.

Godard, M., Bodinier, J.-L., Vasseur, G., 1995. Effects of mineralogical reactions on trace element redistributions in mantle rocks during percolation processes: a chromatographic approach. Earth Planet. Sci. Lett. 133, 449–461.

Godard, M., Jousselin, D., Bodinier, J.-L., 2000. Relationships between geochemistry and structure beneath a paleo-spreading centre: a study of the mantle section in the Oman Ophiolite. Earth Planet. Sci. Lett. 180, 133–148.

Grant, J.A., 1986. The Isocon Diagram—a simple solution to the Gresens' Equation for metasomatic alteration. Econ. Geol. 81, 1976–1982.

Hart, S.R., Zindler, A., 1986. In search of a bulk Earth composition. Chem. Geol. 57, 247–267.

Heling, D., Schwarz, A., 1992. Iowaite in serpentinite muds at Sites 778, 779, 780, and 784: a possible cause for the low chlorinity of pore waters. In: Fryer, P., Pearce, J.A., Stokking, L.B. (Eds.), Proc. ODP, Sci. Repts., vol. 125. Ocean Drilling Program, College Station TX, pp. 313–323.

Ionov, D.A., Savoyant, L., Dupuy, C., 1992. Application of the ICP-MS technique to trace element analysis of peridotites and their minerals. Geostand. Newsl. 16, 311–315.

Jagoutz, E., Palme, H., Baddenhausen, H., Blum, K., Cendales, M., Dreibus, G., Spettel, B., Lorentz, V., Wänke, H., 1979. The abundance of major, minor and trace elements in the Earth's mantle as derived from primitive ultramafic nodules. Proceedings of the Lunar and Planetary Scientific Conference. Geochim. Cosmochim. Acta Supplement, vol. 10, pp. 2031–2050.

Janecky, D.R., Seyfried Jr., W.E., 1986. Hydrothermal serpentinization of peridotite within the oceanic crust: experimental investigations of mineralogy and major element chemistry. Geochim. Cosmochim. Acta 50, 1357–1378.

Jochum, K.P., Seufert, H.M., Thirwall, M.F., 1990. High-sensitivity Nb analysis by spark source mass spectrometry (SSMS) and calibration of XRF Nb and Zr. Chem. Geol. 81, 1–16.

Kelemen, P., Kikawa, E., Miller, D.J., Shipboard Scientific Party, 2004. ODP Leg 209 drills into mantle peridotite along the Mid-Atlantic Ridge from 14°N to 16°N. JOIDES J. 30, 14–20.

Kelemen, P., Kikawa, E., Miller, D.J., Shipboard Scientific Party, submitted for publication. Igneous crystallization and localized deformation in a thick thermal boundary layer beneath the Mid-Atlantic Ridge: Major results from ODP Leg 209. Nature.

Kelley, D.S., Karson, J.A., Blackman, D.K., Früh-Green, G.L., Butterfield, D.A., Lilley, M.D., Olson, E.J., Schrenk, O.M., Roe, K.K., Lebon, G.T., Rivizzigno, P., AT3-60 Shipboard Party, 2001. An off-axis hydrothermal vent field near the Mid-Atlantic Ridge at 30° N. Nature 412, 145–149.

Kelley, D.S., Karson, J.A., Früh-Green, G.L., et al., 2005. A serpentinite-hosted ecosystem: the Lost City hydrothermal field. Science 307, 1428–1434.

Klinkhammer, G.P., Elderfield, H., Edmond, J.M., Mitra, A., 1994. Geochemical implications of rare earth element patterns in hydrothermal fluids from mid-ocean ridges. Geochim. Cosmochim. Acta 58, 5105–5113.

Komor, S.C., Elthon, D., Casey, J.F., 1985. Serpentinization of cumulate ultramafic rocks from the North Arm Mountain massif of the Bay of Islands ophiolite. Geochim. Cosmochim. Acta 49, 2331–2338.

Korotev, R.L., 1996. A self-consistent compilation of elemental concentration data for 93 geochemical reference samples. Geostand. Newsl. 20, 217–246.

Lagabrielle, Y., Bideau, D., Cannat, M., Karson, J.A., Mével, C., 1998. Ultramafic–mafic plutonic rock suites exposed along the Mid-Atlantic Ridge (10°N–30°N)—symmetrical asymmetrical distribution and implications for seafloor spreading processes. In: Buck, W.R., Delaney, P.T., Karson, J.A., Lagabrielle, Y. (Eds.), Faulting and magmatism at mid ocean ridges. AGU Geophysical Monograph, vol. 106, pp. 153–176.

MacLean, W.H., 1990. Mass change calculations in altered rock series. Miner. Depos. 25, 44–49.

MacLean, W.H., Barrett, T.J., 1993. Lithogeochemical techniques using immobile elements. J. Geochem. Explor. 48, 109–133.

Makishima, A., Nakamura, E., 1997. Suppression of matrix effects in ICP-MS by high power operation of ICP: application to precise determination of Rb, Sr, Y, Cs, Ba, REE, Pb, Th and U at ng–g^{-1} levels in milligram silicate samples. Geostand. Newsl. 21, 307–320.

Miyashiro, A., Shido, F., Ewing, M., 1969. Composition and origin of serpentinites from the Mid-Atlantic Ridge near 24° and 30° north latitude. Contrib. Mineral. Petrol. 23, 117–127.

Moll, M., Paulick, H., Suhr, G., Bach, W., submitted for publication. Microprobe data of primary and secondary phases from ODP Sites 1268, 1272, and 1274. In: Kelemen, P.B., Kikawa, E., Miller, D.J., (Eds), Proc. ODP, Sci. Results 209. College Station TX (Ocean Drilling Program).

Mozgova, N.N., Efimov, A., Borodaev, Y.S., Krasnov, S.G., Cherkashov, G.A., Stepanova, T.V., Ashadze, A.M., 1999. Mineralogy and chemistry of massive sulfides from the Logatchev hydrothermal field (14°45′N Mid-Atlantic Ridge). Explor. Min. Geol. 8, 379–395.

Navon, O., Stolper, E., 1987. Geochemical consequences of melt percolation; the upper mantle as a chromatographic column. J. Geol. 95, 285–307.

Niu, Y., 2004. Bulk-rock major and trace element compositions of abyssal peridotites: implications for mantle melting, melt extraction and post-melting processes beneath mid-ocean ridges. J. Petrol. 45, 2423–2458.

Niu, Y., Hekinian, R., 1997. Spreading rate dependence of the extent of mantle melting beneath ocean ridges. Nature 385, 326–329.

Niu, Y., Langmuir, C.H., Kinzler, R.J., 1997. The origin of abyssal peridotites: a new perspective. Earth Planet. Sci. Lett. 152, 251–265.

O'Hanley, D.S., 1996. Serpentinites—records of tectonic and petrological history. Oxford Monographs on Geology and Geophysics, vol. 34. Oxford University Press. 277 pp.

Parkinson, I.J., Pearce, J.A., 1998. Peridotites from the Izu-Bonin-Mariana Forearc (ODP Leg 125): evidence for mantle melting and melt–mantle interaction in a supra-subduction zone setting. J. Petrol. 39, 1577–1618.

Pearce, J.A., Barker, P.F., Edwards, S.J., Parkinson, I.J., Leat, P.T., 2000. Geochemistry and tectonic significance of peridotites from the South Sandwich arc-basin system, South Atlantic. Contrib. Mineral. Petrol. 139, 36–53.

Pin, C., Joannon, S., 1997. Low level analysis of lanthanides in eleven silicate rocks by ICP MS after group separation using cation exchange chromatography. Geostand. Newsl. 21, 43–50.

Robie, R.A., Hemingway, B.S., Fisher, J.R., 1979. Thermodynamic properties of minerals and related substances at 298.15 K and 1 Bar pressure and at higher temperatures. Geological Survey Bulletin, vol. 1452. Unites States Government Printing Office, Washington. 257 pp.

Saccocia, P.J., Ding, K., Berndt, J.S., Seewald, J.S., Seyfried, W.E., 1994. Experimental and theoretical perspectives on crustal alteration at mid-ocean ridges. In: Lentz, D.R. (Ed.), Alteration and alteration processes associated with ore-forming systems. . Short Course Notes, vol. 11. Geological Association of Canada, St John's, Newfoundland, pp. 403–431.

Sauter, D., Mendel, V., Rommevaux-Jestin, C., Parson, L.M., Fujimoto, H., Mével, C., Cannat, M., Tamaki, K., 2004. Focused magmatism versus amagmatic spreading along the ultra-slow spreading Southwest Indian Ridge: evidence from TOBI side sonar imagery. Geochem., Geophys., Geosys. 5, 1–20.

Shannon, R.D., 1976. Revised effective radii and systematic studies of interatomic distances in halides and chalcogenides. Acta Crystallogr. 32, 751–767.

Shipboard Scientific Party, 2004. Leg 209 summary. In: Kelemen, P.B., Kikawa, E., Miller, D.J., et al. (Eds.), Proc. ODP, Init. Repts., vol. 209. Ocean Drilling Program, College Station TX, pp. 1–139.

Snow, J., Dick, H., 1995. Pervasive magnesium loss by marine weathering of peridotite. Geochim. Cosmochim. Acta 59, 4219–4235.

Thompson, G., Melson, W.G., 1970. Boron contents of serpentinites and metabasalts in the oceanic crust: implications for the boron cycle in the oceans. Earth Planet. Sci. Lett. 8, 61–65.

Wicks, F.J., Whittaker, E.J.W., 1977. Serpentine textures and serpentinization. Can. Mineral. 15, 459–488.